INFLUENCE OF SHEARING STRAIN-RATE ON THE MECHANICAL BEHAVIOUR OF THREE STRUCTURED CLAYS

TRUONG LE[*], DAVID AIREY[†] AND JAMIE R. STANDING[*]

[*]Imperial College London
e-mail: truong.le@imperial.ac.uk; j.standing@imperial.ac.uk

[†]The University of Sydney
e-mail: david.airey@sydney.edu.au

Key words: laboratory tests, clays, strain-rate, structure of soils, rate-dependent behaviour

Abstract.

This paper presents the stress-strain behaviour of three structured clays subjected to a number of stepwise changes in strain-rate during shearing in a triaxial apparatus. Undrained compression tests were performed on clay specimens in both undisturbed and reconstituted states. As a result, it has been possible to identify the influence of structure on the rate-dependent response of the clays. Step-changes in applied shearing strain-rates for all tests resulted in predominately isotache-type behaviour within the range of strains from very small strains to large strains at failure. At very small strains, evidence of a limiting elastic modulus was established for both the stiff sedimentary and artificially cemented soil, which is consistent with published literature on other structured geomaterials. The stress-strain behaviour of all three materials was affected by both the degradation of structure with increasing strain and applied strain-rate. The influence of structure on the time-dependent behaviour of the clays is discussed by comparing the response of undisturbed and reconstituted specimens and following normalization by the equivalent pressure. Results indicate that the rate sensitivity evolves with increasing strains and reaches a maximum at strain levels associated with peak shearing resistance.

1 INTRODUCTION

Establishing the appropriate representative stiffness and strength of a soil is fundamentally important when assigning parameters for detailed theoretical or numerical analysis. It is well known that the undrained stress-strain-strength behaviour of a saturated clay is significantly affected by the applied rate of loading. This phenomenon has been studied extensively since the work of Taylor and Merchant (1940) and Casagrande and Wilson (1951). Experimental

data have collectively indicated a consistent relationship between the applied rate of loading and the mechanical response, in particular for (*i*) vertical preconsolidation pressure, σ'_{pc} and (*ii*) undrained shear strength, S_u. The 'isotache model' was subsequently proposed by Šuklje (1957) which uniquely related the one-dimensional volumetric compression curves in $e - \sigma'_v$ space with applied rates of strain (i.e. an independent $e - \sigma'_v$ curve resulted from each strain-rate applied). The importance of rate effects has also been shown in research investigating the time-dependent nature of both reconstituted (e.g. Richardson and Whitman, 1963) and naturally occurring clays (e.g. Berre and Bjerrum, 1973, Sällfors, 1975, Crooks and Graham, 1976, Vaid et al., 1979). The experimental data were subsequently re-assessed by Graham et al. (1988) to form a framework for understanding the stress-strain-volumetric behaviour of a wide range of natural and reconstituted materials based on considerations of yielding. In this way, the effects of time and strain-rate on the preconsolidation pressure and undrained shear strength could be generalised to apply to the entire yield surface. A number of researchers (e.g. Crooks and Graham, 1976, Leroueil et al., 1983, Lefebvre and Leboeuf, 1987) have shown that the variation of the yield stress with log cycle increase in strain-rate is similar across a range of non-organic clays, being approximately 10% per log cycle.

Triaxial tests with a single step-change in shearing strain-rate performed by Richardson and Whitman (1963) on remoulded 'fat' clay demonstrated the rate dependency of the stress-strain curve at different strain levels. Graham et al. (1983) were later able to show, by performing a number of step-changed shearing strain-rate stages, that a unique set of stress-strain curves exist for a given set of axial strain-rates and that the strain-rate history does not have any effect on the stress-strain curve produced from the current applied strain-rate. Momoya et al. (1998) and Tatsuoka et al. (2000) subsequently observed a dependence of the undrained stress path on the applied shearing strain-rate. Tatsuoka et al. (2000) applied the isotache concept to describe the time-dependent stress-strain behaviour of both reconstituted clays and other geomaterials throughout an undrained shearing stage. It is noted that the isotache concept was further developed by Tatsuoka et al. (2002) to account for temporary effects of strain-rate and acceleration (TESRA) observed in a range of sands and some reconstituted clays (e.g. Fujinomori clay). Transitional viscous responses between the isotache behaviour at low stress levels and a combined TESRA and isotache behaviour at higher stress levels have subsequently been observed for a number of other reconstituted natural clays (e.g. Oimachi clay, Komoto et al. 2003.; Fukakusa clay, Oka et al. 2003; London Clay, Sorensen et al. 2007).

From the literature available, it is clear that a large number of experimental investigations into the rate-dependent behaviour (often referred to as viscous effects) of clays have already been carried out on both laboratory reconstituted and undisturbed specimens of natural clays. However, these investigations on the time-dependent behaviour of clays, with a few notable exceptions (e.g. Graham et al., 1983, Locat and Demers, 1988, Boudali et al., 1994, Jeong et al., 2010), involved clays from only one origin and therefore each possessed only a single type of structure. The term 'structure' is defined in this paper as the combination of 'fabric', the arrangement of the component particles, and 'bonding', between particles (Lambe and Whitman, 1969). Only limited studies (e.g. Cotecchia and Chandler, 2000) have compared directly the behaviour of clays with different types of structure, namely 'sedimentation', 'post-sedimentation/diagenesis' and 'bonded/cementation' structures. The influence of the anisotropy and fabric of different natural clays on their time-dependent behaviour has, until recently (e.g. Cotecchia and Chandler, 1997, Sorensen et al., 2007, Jeong et al., 2010, Gasparre et al., 2014), been largely overlooked despite the fact that many of the aforementioned investigations have involved natural clays. Additional experimental data, from shearing different undisturbed structured clays, are therefore needed to establish the interaction between structure and applied shearing strain-rate in order to incorporate correctly any existing data sets into a more generalised time-dependent constitutive framework.

This present study aims to investigate the combined effects of strain-rate and structure on the mechanical behaviour of two natural clays (London Clay and Ballina clay) and one artificially cemented clay (gypsum-kaolin mixture). As highlighted previously by other researchers (e.g. Richardson and Whitman, 1963), significant difficulties can be expected when investigating shearing rate effects on natural soils due to problems associated with sample variability and strain localisation. These can be overcome by applying stepwise changes in strain-rate instead of a constant strain-rate during the shearing phase. A suite of multistage stepwise change in strain-rate tests has therefore been performed on the three different structured clays in both intact and reconstituted states to assess the influence of structure on the rate-dependent behaviour of clays. After presenting the results, the effects of different types of structure on the clays' time-dependent mechanical responses are discussed.

2 TESTING MATERIALS AND SAMPLE PREPARATION

The three clays used in this study were selected as being characteristic examples of (i) a heavily overconsolidated stiff marine clay (London Clay), (ii) a lightly overconsolidated natural estuarine soft clay (Ballina clay) and (iii) an artificially cemented/bonded clay (gypsum-kaolin mixture). All three clays have been previously studied and are recognised as having different soil structure as a result of differences in soil fabric, geological history and degree of cementation (London Clay, Hight et al. 2002, Gasparre et al. 2007; Ballina clay, Pineda et al. 2016b; artificial gypsum-kaolin mixture, Le and Airey, 2021). The geotechnical index properties of the three soils used in this study are listed in Table 1. Short descriptions of the geological history, mineralogy and sample preparation method are provided in the following sections.

2.1 London Clay

Natural London Clay was deposited under marine conditions in the early Eocene sedimentary basin covering much of northern and north-eastern Europe. The soil and surrounding Jurassic shales, Greensand, Chalk and Eocene soils deposited during this period were subsequently eroded to form a very stiff and heavily overconsolidated clay (King, 1981, De Freitas and Mannion, 2007, Gasparre et al., 2007). The clay minerals present in the formation are kaolinite, illite, chlorite, smectite and montmorillonite with trace amounts of pyrite, calcium carbonate and gypsum (Hight et al., 2002, Huggett and Knox, 2006). Sedimentary basins in northern Europe are known to show evidence of vertical and horizontal compression, with the predominant discontinuities being continuous faults of up to several metres length present in these basins (Chandler et al., 2004). The 100-mm diameter undisturbed rotary core samples used in the study were retrieved from Hyde Park, London, as part of an investigation into tunnelling-induced settlements (Wan et al., 2017a, Wan et al., 2017b). The London Clay samples were selected from similar depths, 18.06 - 21.50 m of the Division B2(a) of the London Clay Formation (King, 1981, Standing, 2020). The ends of the undisturbed specimens were trimmed to produce cylinders with diameter of 100 mm and length of 200 mm. The reconstituted specimen of London Clay were created by thoroughly mixing the trimmings of the undisturbed samples with deionised water to a moisture content about 1.5 times the liquid limit and compressed to 200 kPa vertical stress in a 70 mm diameter consolidometer before

trimming and installing in the triaxial apparatus. The vertical effective stress of 200 kPa was chosen to form a specimen with sufficient strength to support the local instrumentation.

2.2 Ballina clay

The high quality specimens of Ballina clay used in this study were taken using Osterberg-type fixed-piston samplers (89 mm diameter, 600 mm effective length) from the National Soft Soil Field Testing Facility at Ballina (New South Wales). Ballina clay is an estuarine soft clay found in the Richmond River valley on the east coast of Australia. Using quantitative X-ray diffraction, Pineda et al. (2016) found the clay to consist of primarily illite, interstratified illite/smectite, kaolinite, amorphous minerals and traces of other minerals including plagioclase, pyrite, mica and calcite. Soils from the Ballina region commonly include organic matter (1-4% OC) and expansive minerals, as well as weak cementation. Two samples of Ballina clay from the same piston tube (6.4-7.0 m depth) were tested in this study and are characteristic of the soft soils found in this area. The undisturbed specimens were hand-trimmed to produce cylinders with diameter of 54 mm and about 108 mm in length.

Samples taken from this soft clay deposit possess an open fabric with a predominance of macro pores of around 1 μm size. Fabric anisotropy was deemed to be absent within the natural samples of Ballina clay (Pineda et al., 2016). As a result of their geological history, the soils exhibit low undrained strength and high compressibility upon yielding (Pineda et al., 2016). Reconstituted specimens of Ballina clay were made from trimmings of the undisturbed sample. A pore fluid containing natural salts of similar electrical conductivity (Sydney Harbour seawater: 37 mS/cm) was used to form a slurry with about 1.3 times the liquid limit. Samples were created by compressing the slurry in a 50-mm diameter consolidometer to about 50 kPa vertical effective stress before trimming to a 100 mm length and transferred to the triaxial apparatus.

2.3 Artificial gypsum-kaolin mixture

The artificially cemented soil was manufactured from commercially available kaolin (Q38) supplied by Sibelco Australia and dental plaster (calcium hemihydrate, a form of underhydrated gypsum). The materials were stored in powdered form and were dry mixed prior to hydration. Following a detailed investigation of the mechanical properties developed with different mixing ratios of kaolin, calcium hemihydrate and water, a dry mixture of 70% kaolin and 30% calcium hemihydrate, with 60% of the total dry mass of added water, was found to produce a

weakly bonded soil (Le and Airey, 2021). The components were mixed to form a homogenous slurry and carefully transferred, avoiding entrapped air, by spatula to a sufficiently long mould of 54 mm or 70 mm diameter. Due to the relatively quick curing time of calcium hemihydrate into gypsum, samples were able to be vertically extruded from the mould, trimmed to the correct 2:1 height-to-diameter ratio, transferred to a triaxial cell and set up under a small effective confining pressure (10 kPa) within an hour of mixing the slurry. The specimens were saturated by slowly ramping the cell and back pressure a total of 500 kPa while maintaining a low constant effective confining stress.

Reconstituted gypsum-kaolin specimens were prepared by crushing cemented specimens prior to sieving through a 300 μm sieve. The powder passing the sieve was then hand mixed with de-ionised water until a slurry at 1.3 times the liquid limit was obtained. The paste was consolidated in a 50 mm consolidometer with a vertical effective stress of about 50 kPa. The specimens were then trimmed to 100 mm length.

3 TESTING PROGRAMME

This paper presents results from eight consolidated undrained triaxial compression tests with stepwise changes in strain-rate on undisturbed samples, as listed in Table 2. A further four consolidated undrained triaxial compression tests on reconstituted samples were performed to assess the influence of structure on the rate-dependent behaviour of clays, as listed in Table 3. Advanced computer-controlled stress path triaxial tests were performed with either stress- or strain-rate controlled loading. The triaxial apparatus were equipped to measure the external axial and volumetric strains developed during the consolidation and shearing stages. In the case of the London Clay specimens and for ICGKVS01 and 02, local axial and radial strains were also measured using miniature linear variable differential transformers (LVDTs) (Cuccovillo and Coop, 1997, Ackerley et al., 2016) with a resolution 0.0001% (strain). Pore water drainage during the consolidation stages was through both the top and base of all the specimens. In the analysis of the triaxial test data, area changes and membrane resistance have been corrected for following the procedures outlined by Lade (2016). Due to the complexity of the deformation pattern observed, no additional area corrections were made to account for the formation of shear planes. The formation of a shear plane is therefore noted in the relevant figures with the response before and after formation being labelled as ‘pre-rupture’ and ‘post-rupture’ respectively.

Specimens of London Clay were additionally fitted with a mid-height pore water pressure probe in order to assess any potential pore water pressure variations over their height. Radial filter paper strips were also attached to the specimen to accelerate pore pressure equalisation. Both samples of London Clay were consolidated to their in-situ stress state following approach paths that reproduced the site's recent geological history of erosion followed by terrace gravel deposition, referred to by Gasparre et al. (2007) as a "short geological stress path". Mid-height pore water pressures were maintained to be within 5% of the specified back pressure during the consolidation stages. After arriving at the desired effective stress state, the pore pressures were allowed to equilibrate (taking approximately 5-7 days) before moving on to the next consolidation stage. In these tests, the effective stress was calculated based on the mid-height pore water pressure reading. To quantify the influence of post-sedimentary structure on rate-dependent response of London Clay, the reconstituted specimen was consolidated to an isotropic effective stress of 400 kPa where it is known to be on the normally consolidated line.

Due to the relatively young geological age of the Ballina clay and its low in-situ stresses, one specimen was consolidated directly to its in-situ stress state by applying a deviator stress at constant confining pressure ($\Delta q/\Delta p' = 3$) from an appropriate isotropic stress state. However, as the initial in-situ stress state of Ballina clay lies relatively close to the failure envelope (Pineda et al., 2016), an additional test was performed from a higher isotropic stress state to obtain more information about the stress-strain and strain-rate response. This stress state was chosen to be within the gross yield locus identified by Le et al. (2018). The reconstituted sample of Ballina clay was isotropically consolidated to the same isotropic effective stress as for BC6.7VS2 (40 kPa) in order to quantify the contributions of structure on its mechanical behaviour.

All specimens of gypsum-kaolin were consolidated to a common isotropic effective stress of 40 kPa prior to shearing. The initial isotropic stress state was within the yield locus identified by Le and Airey (2021) for the intact material. The reconstituted specimens were also consolidated to the same isotropic effective stress.

All specimens were continuously monitored throughout the consolidation stage and left to rest at a constant effective stress until axial creep strain-rates became negligible prior to undrained shearing. Undrained shearing was controlled using a feedback loop from the load cell or displacement transducer to maintain a specified rate of deviator stress or axial strain increase respectively. Stress-rate control was only defined for a limited number of stages within

the small-strain region to allow the small-strain stiffness trends and effective stress paths to be captured reliably. Reported strain-rates during stress-rate control were obtained by linear regression of the change of strain with time response.

For both the Ballina clay and gypsum-kaolin (except ICGKVS02) specimens, the axial creep strain-rate prior to shearing, $\dot{\varepsilon}_c$, was below 1/100th of the initial axial shearing strain-rate, $\dot{\varepsilon}_a$. As the specimens of London Clay and ICGKVS02 were sheared at very slow shearing rates, a smaller axial shearing strain-rate/creep strain-rate ratio ($\dot{\varepsilon}_a/\dot{\varepsilon}_c$), henceforth referred to as the creep rate ratio, was measured during the first stage of shearing. For the three tests, a minimum value of 4 was measured for the creep rate ratio. The values of axial creep strain-rate prior to shearing for each specimen are listed in Table 2. The creep rate ratios of all reconstituted specimens was above 100; the values of axial creep rate, $\dot{\varepsilon}_c$, and axial strain-rate, $\dot{\varepsilon}_a$, are listed in Table 3. A wide range of strain-rates were applied and varied over two to three orders of magnitude for each test. Strain-rates for all tests were within the range of 0.00038%/hr to 50%/hr. The time for more than 90% internal pore pressure homogenization over the specimen height, during shearing, can be estimated as $t = L^2/c_v$ where L is the maximum drainage length; and c_v is the coefficient of consolidation (Blight, 1964). Taking a nominal axial failure strain of approximately 5%, the time to reach failure can be calculated for each soil at the different strain-rates. The comparison between the internally and externally imposed time-scales suggests that the effective stress within the sample may be non-uniform for stages which had applied the highest strain-rate of 50%/h. It is however expected that the calculated effective stress following a reduction in strain-rate is reliable as pore pressures are allowed to equilibrate.

The stress-strain response is however not likely to be affected by this boundary phenomenon. It is therefore possible that characteristic curves in the stress-strain space can then be interpolated between measured periods for each of the individual strain-rates. The stress-strain relations and effective stress paths are studied here in order to examine the influence of shearing strain-rate on different structured clays.

4 EXPERIMENTAL RESULTS

4.1 London Clay

The tests aimed to investigate the behaviour of undisturbed specimens at small and large strains by evaluating the elastic stress-strain response as well as the shearing strain-rate dependency of the specimens at different strain levels. Results from both samples (LCUB21

and LCUB18) are analysed over the small and large strain ranges, in conjunction with the effective stress paths. For clarity, results for sample LCUB21 are plotted in Figures 1 to 4 and results for sample LCUB18 are plotted in Figures 5 to 8. The values of stress- and strain-rates applied in each test are listed in Table 2.

Similar to other studies on the effects of shearing strain-rate (e.g. Tatsuoka and Shibuya, 1992), the rate-dependent nature of the stress-strain curve was found to differ between the small and large strain levels. At all strain levels, interpretations of strain-rate behaviour were established by connecting the segments of the stress-strain relation with the same strain-rate. Results from the series of curves at different strain-rates reveal that the mechanical behaviour of London Clay can be described as strain-rate dependent at every strain level. The effects of applied strain-rate were more apparent at larger strain levels. Similar to the work carried out by Gasparre et al. (2014), the initial stages of undrained shearing were stress-rate controlled to allow the small-strain stiffness trends and effective stress paths to be captured reliably. As LCUB21 was fitted with a higher sensitivity load cell (5 kN with a resolution of 0.1 N), stress-rates were additionally step-changed to investigate the effects of stress-rate on small-strain stiffness. With the higher resolution in the load cell, the system was able to control reliably the stress-rate at 0.66 and 1.29 kPa/hr, corresponding to strain-rates of approximately 0.00038 to 0.00075%/hr. As LCUB18 was fitted with a higher capacity load cell (10 kN with a resolution of 1 N) only a single stage at 3.3 kPa/hr, corresponding to approximately 0.0016%/hr, was achieved in the very small strain range.

Due to the stiff nature of the London Clay, the strain-rate varied in proportion to the defined stress-rate. Shearing was switched to displacement rate control at a very small axial strain as indicated in Figures 1 and 5. The tangent stiffness increased for LCUB21 when transitioning from stress-rate to strain-rate control where the applied strain-rate increased by two orders of magnitude, whereas no significant change in stiffness was found for LCUB18 when the strain-rate only increased by a single order of magnitude. Undrained compression stages with a creep rate ratio less than 50 has been suggested to cause stiffness ‘under-estimation’ (Gasparre et al., 2014) and in the current tests this is possibly contributing to the different small-strain stiffness values between the two methods of shearing control (stress-rate and strain-rate control) in sample LCUB21. As noted previously, a marked jump in the strain-rate was measured at the transition between the modes of shearing. As the effects of applied shearing strain-rate and creep rate ratio overlap for tests employing stepwise changes in strain-rate, it is not possible to

separate the impact of these two variables. It is evident however that as applied strain-rate decreases and approaches the initial axial creep rate, the measured stiffness reduces. A similar result has been reported by Sorensen et al. (2010) for reconstituted London Clay subjected to different magnitudes of strain-rate 'acceleration' (equivalent to creep rate ratio). Apparatus compliance and specimen contact/bedding imperfections are believed to have not significantly affected the results as measurements were made locally on the samples and strain-rates were calculated from local transducers.

For both samples LCUB21 and LCUB18, a near constant tangent stiffness was found for stages of strain-rate control loading within the small-strain region ($\varepsilon_a < 0.02\%$) as shown in Figures 2 and 6. That is, the stress-strain response continued to be linear despite changes in strain-rate. This behaviour is especially evident in Figure 2, where changes in strain-rate between 0.002 to 0.02%/hr resulted in no measurable deviation in the linear stress-strain response. The linear response of the specimens suggests that in the very small to small strain region, a maximum limiting stiffness can be identified and that the stress-strain response appears to be strain-rate independent for strain-rates above a threshold. Gasparre et al. (2014) found a similar unique undrained elastic modulus for a set of three different strain-rates (0.025, 0.5 and 0.25%/hr) in the range of 0 to 0.05% axial strain.

Following the stages of stress-rate control, both samples of London Clay were sheared to failure with stepwise changes in strain-rate. The overall stress-strain responses and stress paths are shown in Figures 3 and 4 respectively for Sample LCUB21 and Figures 7 and 8 respectively for Sample LCUB18. The stress-strain response was found to be stiff and strain hardening until a peak shear strength where localisation of the strains occurred as a result of the formation of shear planes. For both samples, the peak strength occurred at about 2% axial strain, after which the resistance for LCUB18 dropped off to an ultimate shear strength at larger strains. The formation of a shear plane was noted by visual inspection to have occurred around the peak shear response and to have clearly propagated through the sample by 5-6% axial strain.

In the medium to large strain range (ε_a > 0.1%), stepwise changes in strain-rate resulted in the first observable persistent change in shearing resistance, typical of isotache-type behaviour (curves traced by stages of equal strain-rate), as is evident from Figures 3 and 7. In order to investigate the influence of strain-rate ratio between stages ($\dot{\varepsilon}_{after}/\dot{\varepsilon}_{before}$), the magnitude of strain-rate ratio was varied between the two tests. Stepwise changes in strain-rate were varied by an order of magnitude between each stage for sample LCUB21, whereas strain-rate was

stepped by a factor of two (doubled or halved) between each stage for sample LCUB18. As shown in Figures 3 and 7, the magnitude of the strain-rate ratio directly influences the separation of isotache curves traced by stages of constant strain-rate. The isotache curves increase in separation with increasing strain-rate ratio and strain level. Unique stress-strain isotache curves are observed for different strain-rates in both samples until termination at large strains.

Undrained effective stress paths in $q - p'$ stress space are plotted in Figures 4 and 8 for samples LCUB21 and LCUB18, respectively, at all stages of shearing. Overall, the effective stress response of both samples was consistent with other investigations on natural, structured London Clay (e.g. Bishop et al., 1965, Hight et al., 2002, Hight et al., 2007). That is, a constant stress gradient ($\Delta q/\Delta p'$) is traced from the in-situ stress state until the sample exceeds the very small strain region where the rate of pore pressure generation reduces. With continued strain, the effective stress path of both samples reached a peak stress ratio, $\eta = q/p'$, of approximately 1.4 before reducing to an ultimate, post-rupture stress ratio, as shown in Figure 9. The post-rupture stress ratios are in broad agreement with the ultimate state stress ratio identified by Hight et al. (2007) for undisturbed specimens from Division B2(a) of the London Clay Formation at Heathrow Terminal 5, London. As London Clay is heavily overconsolidated, the point of yielding is on the 'dry side' of the state boundary surface.

For natural specimens of London Clay, stepwise changes in strain-rate are shown to affect the effective stress path both pre- and post-peak (Figures 4 and 8). From the in-situ stress state, as the specimen is sheared, the stress path moves towards a peak shear stress and stepwise changes in strain-rate are found to shift the stress path between isotache lines in $q - p'$ space. For sample LCUB21, where strain-rates were changed by an order of magnitude between stages, the effective stress path was found to move upwards with increases in strain-rate (Figure 4). The effect of stepwise changes in strain-rate is less pronounced for sample LCUB18 as a result of the smaller strain-rate ratio between stages; no noticeable change in stress path was found in the small strain region with changes in strain-rate. Strain-rate sensitivity was more evident as the effective stress path approached the peak stress ratio.

The pore water pressure responses for both samples during undrained shearing are shown in Figure 10. Results suggest that changes in strain-rate do not significantly affect the generation of excess pore pressure until beyond the small strain region. Where strain-rate effects were observed, at large strains and following the formation of a shear band, the excess

pore-water pressure changed proportionally with the strain-rate and persisted through the stage. This resulted in the effective stress paths clearly displaying isotache-type curves between stages of equal strain-rate. Isotache curves for the effective stress path were observed for both specimens until large strains ($\varepsilon_a > 5\%$).

In order to identify the effect of the natural structure on mechanical behaviour, the shearing data from the undrained triaxial tests on both natural and reconstituted samples have been normalised for volume with respect to an equivalent pressure, p'_e, for a given void ratio on the intrinsic isotropic normal compression line (ICL). The intrinsic compression parameters defined by Chen (2014) on nearby samples, given in Table 3, have been used to normalise the effective stress response and. The normalised effective stress paths for both undisturbed samples as well as the normally consolidated reconstituted sample are given in Figure 11. The intrinsic state boundary surface (SBS) identified by Gasparre et al. (2007) is also shown for comparison. As would be expected for a highly overconsolidated clay, the peak states plot significantly higher than the intrinsic SBS for the undisturbed specimens. The normalised undrained stress path for the reconstituted specimen followed the Roscoe-Rendulic surface. The normalised effective stress path for the reconstituted sample was significantly more affected by strain-rate effects than the undisturbed samples. The pore pressure response to changes in axial strain-rate, as shown in Figure 10, was persistent for both the undisturbed and reconstituted samples at low axial strain levels (<0.5%), although it affected the undisturbed samples to a lesser extent. Results for both undisturbed and reconstituted samples reveal the same isotache-type behaviour at all strain levels during shearing.

4.2 Ballina clay

Two triaxial tests with stepwise changes in shearing strain-rate were performed on natural samples of Ballina Clay from a depth of approximately 6.7m below ground level. Table 2 summarises the initial stress states and strain-rates applied. As described earlier, two different initial stress states were selected for tests on Ballina clay due to the proximity of the in-situ stress state to failure envelope. Sample BC6.7VS1 was anisotropically consolidated to the estimated in-situ stress state while sample BC6.7VS2 was isotropically consolidated to 40 kPa. Figure 12 presents the stress-strain curves from subsequent shearing of the Ballina Clay. Due to the difference in initial stress state, the strains at the peak shear stress are noticeably different

between the two samples, being about 0.7% and 4% axial strain for BC6.7VS1 and BC6.7VS2 respectively.

From both an anisotropic and isotropic stress state, stepwise changes in strain-rate are seen to vary the measured shearing resistance. Stepwise changes in strain-rate for the isotropically consolidated sample of natural Ballina Clay (BC6.7VS2) result in isotache behaviour with distinct and persistent variations in shearing resistance throughout the loading stage. For the anisotropically consolidated sample (BC6.7VS1), stepwise changes in strain-rate result in smaller jumps in shearing resistance, especially in the strain range of 0 to 2%. Despite both tests starting from inside the gross yield surface, the responses were influenced by the relative proximity of the initial stress state to failure. Specifically, when the initial in-situ stress state was close to yield, this reduced the strain range prior to yielding, thereby suppressing evidence of rate-dependent behaviour as the natural structure collapsed almost immediately upon shearing. Despite this, isotache-type behaviour was evident for both samples but was more apparent for sample BC6.7VS2 where stepwise changes in strain-rate were performed within the gross yield surface and away from the failure envelope.

Figure 13 shows the effective stress paths for the two stepwise change in strain-rate tests on Ballina clay. Upon undrained compression, both samples followed a path of constant stress gradient $\Delta q/\Delta p' \approx -2.9$ until reaching the peak stress ratio ($\eta = 1.80$), which is then followed by gradual structural collapse until reaching an ultimate stress ratio of approximately 1.46. A persistent pore pressure response to changes in axial strain-rate, as shown in Figure 14, was observed for both undisturbed samples. Interestingly, this resulted in the effective stress path experiencing minimal translation with changes in strain rate prior to peak (Figure 13). However, after reaching the peak strength envelope, the effective stress paths did respond to changes in strain-rate. The effective stress paths and ultimate failure envelope of both samples are consistent with those presented by Pineda et al. (2016) for samples from a similar depth. Due to the low effective confining pressures measured for 6.7VS1 in compression, excess pore pressure readings beyond 5% strain were deemed unreliable. Both samples were seen to barrel with no observable shear band formed as a result of shearing to large strains.

The undrained compression behaviour of a reconstituted sample of Ballina clay was also investigated to establish the contributions of structure to the rate dependent response of a soft clay. The results for the reconstituted sample are also shown in Figures 12 to 16. A comparison of the responses of the two samples, 6.7VS2 and r6.7VS, which were consolidated to a common

isotropic effective stress, reveals that the undisturbed sample failed at a higher peak stress ratio but reduces to a common critical state stress ratio (M=1.462) with continued strain, as would be expected. Changes in strain-rate also affected the effective stress path of the reconstituted sample more significantly than that of the undisturbed sample, suggesting that the effective stress path sensitivity is linked to the structure for a soft clay. Stepwise changes in strain-rate resulted in persistent changes in the measured stress ratio for both the undisturbed and reconstituted specimens, as shown in Figure 15. Normalisation for volume with respect to an equivalent pressure on the isotropic NCL determined for the reconstituted clay, indicates that Ballina clay has a stress sensitivity, $S_\sigma = p'/p'_e \approx 3.5$, similar to that of other soft clays (e.g. Bothkennar clay (≈ 4), Smith et al., 1992). The normalized stress paths of both the natural and reconstituted samples, shown in Figure 16, are bounded by a common peak and ultimate strength envelope. Similar to Bothkennar clay, undrained shearing after reaching the intact strength envelope leads to a loss of structure with the normalised effective stress path heading towards the intrinsic SBS. Assuming the normalised effective stress path is on the intact SBS at the peak shearing resistance, changes in strain-rate result in the expansion or contraction of the SBS with an increase or decrease in strain-rate respectively. A comparison of the SBS for the undisturbed and reconstituted samples suggests that (i) the natural structure allows for a higher peak strength envelope to be reached by the undisturbed sample, as would be expected, (ii) the peak strength envelope appears to be dependent on the axial shearing strain-rate and (iii) strain-rate effects are persistent at all strain levels for both undisturbed and reconstituted samples of Ballina clay.

4.3 Gypsum-kaolin specimens

The effect of stepwise changes in strain-rate tests on four gypsum cemented kaolin samples were investigated in this study. All four specimens were consolidated to the same initial isotropic stress state within the yield locus as listed in Table 2. Figures 17(a) and (b) shows the stress-strain curves obtained for the intact gypsum-kaolin specimens during shearing in undrained compression at small and large strain, respectively. As ICGKVS02 was also fitted with local instrumentation, slower stress-rate control stages were defined to investigate the rate-dependence at small-strains. The variability in peak shearing resistance reflects the recognised difficulty in preparing artificially cemented samples at the same void ratio. Nevertheless, the axial strain-rate sensitivity of the stress-strain behaviour is consistent, as will

be shown, despite the scatter in peak shear strength values. Stepwise changes in shearing strain-rate tests on the gypsum-kaolin specimens resulted in similar stress-strain responses to those performed at constant strain-rate tests (Le and Airey, 2021), the bounds of which are given by the grey shaded area. Similar to the constant strain-rate tests, the samples exhibit a very stiff elastic type response until reaching a peak shear stress at an axial strain of approximately 0.5 to 1.0%. The stress-strain behaviour then subsequently softens with strain following the peaks as shear bands formed through the samples. The strain at which shear bands formed could not be confirmed for ICGKVS01 and 02 as the confining cell was made of steel but multiple shear planes were observed at the end of the tests. Rupture was therefore assumed to occur at a similar strain level as those found for GKVS03 and 04, at about 1% axial strain. Results are again separated into either pre- or post-rupture to highlight the formation of shear bands in the test specimens.

A unique small strain stiffness value could be determined for ICGKVS01 and 02 due to the availability of local instrumentation. The range of strain for which the maximum stiffness value was measured is shown to depend on applied strain-rate, with a greater elastic strain region for the faster strain-rate. Within the small-strain region, the stress-strain curve for the sample sheared at a slower rate, under stress-rate control, is noticeably softer (ICGKVS02) than for the sample sheared at a constant rate of strain (ICGKVS01). The results from GKVS03 and GKVS04 are included but are not discussed in detail as axial strains were determined using external displacement transducers.

At larger strains, stepwise changes in strain-rate resulted in well defined stress-strain isotache curves, as would be expected. Similar to the observation made by Richardson and Whitman (1963), stress-strain curves from constant strain-rate tests did not coincide directly with those derived between stages performed with stepwise changes in strain-rate, which may be attributed to sample variability evident in the scatter of initial void ratio. Three key rate-dependent effects are still observed for the cemented material: (i) there is a clear similarity in rate sensitivity for the stress-strain curves prior to and following the peak undrained shear strength for all strain-rates applied, (ii) changes in undrained shearing resistance are observed to be proportional to changes in strain-rate and (iii) the stress-strain response appears to be characteristic of isotache behaviour at all strain levels. The stress-strain response of the intact material is typical of a structured soil with a clear peak followed by a rapid loss of strength.

The stress-strain curves then soften towards a non-unique deviatoric stress level, consistent with the behaviour observed from constant rate of strain tests reported by Le and Airey (2021).

Figures 18 and 19 show the effective stress paths and variation of stress ratio with axial strain for the intact gypsum-kaolin samples. The effective stress response of the four samples agrees broadly with the bounds presented by Le and Airey (2021) for tests with constant strain-rate, shown as the grey shaded area. The stress ratio of the samples is shown to reduce with increasing strain after the peak which was reached at about 0.5-1% strain. The lower peak stress ratios reached by ICGKVS01 and 02 are attributed to different values of initial void ratio (Table 2). The difference in peak response appears however to have minimal impact on the variation of stress ratio with axial strain prior to peak. Unlike the undisturbed natural soils, stepwise changes in strain-rate resulted in persistent changes in the effective stress path and stress ratio during shearing in undrained compression, with increases and decreases shifting the effective stress state to the right and left respectively. Following the very slow shearing associated with stress-rate control, the increase in strain rate (shown as point A in Figure 18d) resulted in a near vertical effective stress path before reaching the stress path traced by ICVS01 which was subjected to a similar strain-rate. The effective stress responses of all four samples show signs of structural degradation at strains beyond peak, although no common stress path could be determined post-rupture. The pore pressure responses for the intact samples during undrained compression are shown in Figure 20. At both small and large strains, changes in strain-rate correlate with small temporary changes in pore pressure, and pore pressures are considered to be independent of axial strain-rate. The responses in terms of stress-strain, effective stress path and pore pressure indicate that the cemented gypsum-kaolin samples exhibit typical isotache-type behaviour. The insensitivity of the pore pressure suggests that the rate-dependency is associated with the relatively stiff soil matrix and is independent of drainage.

The sensitivity of both the stress-strain and effective stress paths to initial void ratio is confirmed by comparing the normalized stress paths, as shown in Figure 21. Due to the high stress sensitivity (p'/p'_e) for the soil, slight variability in initial void ratio significantly affects the location of the normalised stress path. The paths of all four samples did however approach a common maximum strength envelope at peak. Samples with lower initial void ratio, thereby having a lower initial p'/p'_e value, exhibited a higher peak shearing strength, shown previously in Figure 17 (b).

Results from two reconstituted gypsum-kaolin mixtures are presented to quantify the contributions of cementation on the observed rate-dependent behaviour. The results obtained for the reconstituted samples are presented in Figures 17-20 for comparison. Similar to the intact specimens, isotache-type behaviour is evident in the stress-strain and effective stress paths when subjected to changes in strain rate. These effects were persistent and present at all strain levels. The pore pressure responses of the reconstituted samples were also insensitive to changes in strain rate. The influence of structure on the mechanical response is clear when comparing results from the intact and reconstituted specimens. Strain-rate dependence was significantly affected by the removal of structure.

5 DISCUSSION

5.1 Stress-strain sensitivity to strain rate

The mechanical responses of the three structured soils all showed a sensitivity to axial strain-rate. The effects of changes in strain-rate were found to be similar between the soils in the intact and reconstituted states. Results from both the stiff overconsolidated clay (London Clay) and bonded soil (gypsum-cemented kaolin specimens) were found to support the concept of an elastic limit line (ELL) originally hypothesised by Tatsuoka and Shibuya (1992). In terms of stiffness, the maximum value on the limiting line is the initial tangent stiffness at small strains, which is constant within an 'elastic' zone, beyond which it starts to reduce. Internal instrumentation has shown that provided the strain-rate is above some critical value, changes in rate do not have noticeable effects on the stress-strain response within the 'elastic' zone. Experimental evidence for this is shown in Figure 5(a) where the stress-strain response remains constant even though the strain-rate is changed by an order of magnitude. However, the experiments also show that for stiff soils, the point at which the stiffness reduces from the maximum initial value ($E_{u,max}$) depends on the applied strain-rate. As the strain-rate increases, the $E_{u,max}$ stiffness is maintained to larger axial strains. At very low strain-rates, the elastic region is greatly reduced, with a deviation of the stress-strain curve from the ELL occurring from the onset of shearing, despite being within the typical strain-rate independent strain levels.

To facilitate this concept, a hypothetical schematic of the stiffness decay curves for tests of constant strain-rate ($\dot{\varepsilon}_0$ to $\dot{\varepsilon}_4$ from slowest to fastest) is plotted in Figure 22. As described by the elastic limit line hypothesis, the strain extent of the elastic limit is shown to be strain-rate dependent but the stiffness is limited to a maximum value, $E_{u,max}$. This maximum stiffness

value is the same for strain rates $\dot{\varepsilon}_1$ to $\dot{\varepsilon}_4$ and is maintained to greater strain levels as the strain rate increases (e.g. from $\dot{\varepsilon}_1$ to $\dot{\varepsilon}_4$ with associated strains of about 0.002% and 0.025% respectively).

The stress-strain response for test LCUB21 shows the existence of the previously hypothesised lower bound stiffness, $E_{u,min}$ (Di Benedetto and Tatsuoka, 1997). Two different, but near constant, Young's modulus values can be determined for the very slow and slow strain rates. As shown in Figure 1a, a lower stiffness is measured while under stress rate control and is relatively constant even though the associated strain-rate is changed four times. By applying a faster strain-rate, a higher, but also constant, stiffness is measured. At higher strains, such as point A in Figure 2(a), isotache-type behaviour first becomes evident and a decrease in strain-rate results in a drop in deviator stress (from A to B) as the stress-strain curve collapses onto the isotache curve associated with the slower applied strain-rate. At point C (also shown in Figure 2), a subsequent increase in strain-rate results in the deviator stress increasing along a pseudo-elastic limit line until the stress-strain response re-joins the isotache curve associated with the higher strain-rate, as described above. This experimental evidence is the first which clearly demonstrates the existence of multiple isotache curves at small strains.

An associated minimum stiffness is also plotted in Figure 22 which corresponds to a sample where an extremely slow strain-rate is applied during shearing. The influence of the creep rate ratio, $\dot{\varepsilon}_a/\dot{\varepsilon}_c$, on the mechanical response at standard rates of shearing has been studied in detail by Clayton and Heymann (2001). Results from this current study, which were performed at much slower rates of shearing, suggest that the maximum stiffness is only measured when the residual creep rate is sufficiently smaller (<1/20th) than the applied shearing rate. The creep rate ratio is thought not to affect the extent of the elastic limit, however further investigation is needed to examine this phenomenon as well as the minimum elastic limit.

At medium and large strains, isotache-type behaviour is better understood and has been described in detail by a number of authors (e.g. Leroueil, 2006, Tatsuoka et al., 2008). Typically, a material is defined as having isotache viscosity when the current stress value is a unique function of the instantaneous strain and strain-rate irrespective of the preceding strain history. The stress-strain curves of different constant strain-rates are often similar in form and are related by a logarithmic strain-rate function. All three structured clays were shown to display isotache-type behaviour at medium to large strains despite the uncertain interpretation of stresses and strains after the formation of shear planes.

5.2 Effective stress path sensitivity to strain rate

Complex rate-dependent behaviour has also been shown to exist for all soils in effective stress space (e.g. stress paths in $q - p'$ space). Generally, stepwise changes in strain-rate result in the effective stress path shifting between isotache-related curves, similar to the stress-strain behaviour. The nature of the isotache behaviour in effective stress space was not unique among the soils investigated. As the stress-strain responses of each soil were found to show isotache-type viscosity, the persistence of changes in pore pressure affected the separation of isotache responses of the undrained effective stress paths. Where only relatively small changes in pore pressure response were recorded, clear isotache curves could be traced in the effective stress space. Isotache curves in effective stress space were not readily identified for the soft Ballina clay prior to peak as a result of the interaction between excess pore pressure generation and shear stress development. The axial strain-rate sensitivity of the effective stress path was found to be most significant in the cemented soil while both the undisturbed stiff overconsolidated clay and soft clay showed significantly less separation of the isotach curves. A similar insensitivity of the initial stress path to applied strain-rate is presented by Smith (1992) and Hight et al. (1992) for Bothkennar clay.

Persistent changes in stress ratio, characteristic of isotache behaviour, were found for all three structured soils with different stress ratio responses for different strain rates. The measured peak stress ratio was therefore found to be rate sensitive for all soils. The effects of structural collapse are seen in the reduction in stress ratio towards an ultimate value.

5.3 Influence of structure

The influence of structure on both the stress-strain and effective stress responses is evident for all three soils. Similar to many other naturally structured soils (e.g. Leroueil and Vaughan, 1990, Burland et al., 1996, Cotecchia and Chandler, 1997), data presented for the three intact soils show well-defined peak strength envelopes and progressive loss of structure with post-yield strain. A comparison of the behaviour between the intact structured and the reconstituted specimens shows that the destructured clays are less stiff and reach smaller peak strengths at large strains. The maximum stress ratios for the reconstituted specimens were achieved at large strains, without an apparent yield stress, and generally corresponded to the ultimate stress ratio of the intact undisturbed soils.

Although the structure present in the soils investigated are different in nature, the strain-rate sensitivities of all three soils are similar. Isotache-type behaviour was identified in all samples prior to peak, irrespective of the type of structure. The influence of destructuration on the type of viscous behaviour exhibited by the soils was minimal as isotache curves could be traced for both the intact and reconstituted soils. This would suggest that rate-dependency is preserved despite changes in the degree of structure. The effect of mineralogy on rate-sensitivity is difficult to quantify as the clays are of different origins and have a range of stress histories. It can however be said that the data presented indicate that the effects of strain-rate on structured soils can be interpreted within a common framework which considers the behaviour of soils in the intact and reconstituted states. The nature of the structure did however affect the relative change (degree of rate-sensitivity) in shearing resistance with axial strain-rate. Two methods of interpreting the strain-rate sensitivity of structured clays are now presented.

5.4 Interpretation of rate effects using a rheological framework

The effect of stepwise changes in strain-rate on the stress-strain behaviour can be quantified by measuring the strain-rate ratio ($\dot{\varepsilon}_{after}/\dot{\varepsilon}_{before}$) against normalized shearing resistance, $\Delta q/q^*$, where Δq is the vertical distance between two isotache curves at the instance where a step change in $\dot{\varepsilon}$ occurs and $q^*(= q - q_0)$ is the change in deviator stress from the beginning of the shearing phase (shown in Figure 3). A plot of this relationship for the three soils is shown in Figure 23(a). Di Benedetto et al. (2002) and Tatsuoka et al. (2002) proposed that the rate sensitivity relationship can be expressed by a semi-logarithmic function of type

$$\frac{\Delta q}{q^*} = \beta \cdot \log_{10}\left(\frac{\dot{\varepsilon}_{after}}{\dot{\varepsilon}_{before}}\right) \quad (1)$$

where β is defined as a 'rate-sensitivity coefficient'. In this investigation, deviator stress, q, was chosen as the measure of shearing resistance as the evolution of the effective stress ratio, η, which was used by Di Benedetto et al. (2002) and Tatsuoka et al. (2002), has been shown to depend on the soil type and the use of the principal effective stress ratio, $R = \sigma'_v/\sigma'_h$, as suggested by Tatsuoka et al. (2008), was not straightforward due to the different initial stress states. A relative difference between the current and initial stress state was therefore found to be more useful as a means of normalizing test results, particularly for tests where the effective stress space passes through the isotropic axis. A new method of presenting the strain-rate relationship is therefore presented, as given in Equation (1). Using the new expression, a

reasonable fit can be obtained with a single β value throughout the shearing phase for each soil, similar to the results of Tatsuoka et al. (2008). The rate-sensitivity coefficients are subsequently determined for the reconstituted soils, as shown in Figure 23(b). A comparison of the corresponding β value for each soil indicates that structure influences the vertical separation of isotache curves in stress-strain space. The removal of structure was found to result in a significant increase, about a two-fold difference, in β value for both natural soils. Interestingly, the β value was found to decrease for the cemented soil with the destruction of structure suggesting that the nature of rate-dependency is dependent on the type of fabric and, if present, cementation.

5.5 Interpretation of rate effects using a rate power law

An alternative method of interpretating rate-sensitivity is to investigate the relative change in deviator stress with strain-rate (e.g. Leroueil et al., 1985, Soga and Mitchell, 1996, Qu et al., 2010). In this approach, strain-rate sensitivity is evaluated using a power law of form

$$\log(q) = \alpha \log(\dot{\varepsilon}_a) + A \qquad (2)$$

where α is the viscosity index and A is a model constant. While this approach is known to be limited due to the a priori assumption of isotache-type behaviour, it was found to provide useful insights into the evolution of rate sensitivity with strain. Figures 24-26 summarise the evolution of the viscosity index α, with strain level for the three structured soils in both the intact and reconstituted states. Three significant observations are made by comparing the viscous index for the intact and reconstituted materials (i) rate sensitivity for structured soils is strain level dependent and was found to have a maximum value at about the strain level associated with peak strength, (ii) the rate sensitivity is not necessarily equivalent for the intact and reconstituted samples and (iii) a minimal change in rate sensitivity was found for the reconstituted soils with strain level. Interestingly, the maximum viscosity index estimated from the intact samples was essentially the same for the reconstituted material. The comparison of rate sensitivity for the intact and reconstituted data at large strains results in a similar relationship obtained from using the rheological approach, that is, rate sensitivity appears to increase for the reconstituted natural soils and reduce for the reconstituted cemented soil. Interpretation of rate-sensitivity using relative change in deviator stress with strain-rate has therefore shown that the persistent effects is indeed affected by structure and that strain-rate sensitivity is at a maximum at about peak shear strength.

6 CONCLUSIONS

The sensitivity of structured clays to changes in strain-rate during undrained shearing in compression in a triaxial apparatus has been investigated. The data presented in this paper form a comprehensive set of results for the axial strain-rate-dependent behaviour for three structured soils from different origins. Stepwise strain-rate tests were performed on both intact and reconstituted specimens to quantify the effects of structure and axial strain-rate on the observed mechanical response. Rate sensitivity was observed irrespective of the nature of the structure present in the specimen. It was found that isotache-type viscosity was applicable for all three soils in both the intact and reconstituted states in stress-strain space. An interaction between structure and strain-rate effects was found to limit generalizing isotache type behaviour in $q - p'$ effective stress space. Significantly, the effective stress paths for the undisturbed natural specimens were found to be relatively insensitive to changes in strain-rate suggesting that the natural structure has more of an impact on the inclination of the stress path than strain-rate.

The change of deviator stress normalized by the total change in deviator stress with logarithmic changes in strain-rate was found to be well approximated by a semi-logarithmic relationship for a range of step sizes for a given soil. An alternative approach, using a rate power law, was also found to model adequately the data, given that only isotache type behaviour was observed. Structure was found to impact the rate sensitivity of all three soils using either approach. A new, but logical, interaction between rate sensitivity and strain level (or structure) is highlighted in this study.

7 ACKNOWLEDGEMENTS

Tests were performed both at the University of Sydney and Imperial College, London. The authors are grateful for the help provided by the technicians at both universities, especially Mr. Ross Barker and Mr Steven Ackerley for their help in setting up the apparatus for the experimental work.

NOTATION

c_v	coefficient of consolidation
$E_{u,tan}$	tangent undrained stiffness at small strains
$E_{u,max}$	maximum undrained stiffness at small strains
$E_{u,min}$	minimum undrained stiffness at small strains

e	void ratio
K_0	coefficient of earth pressure-at-rest
L	drainage length
M	critical state stress ratio
m	rate of change of strain-rate with logarithmic time
p'	mean effective stress
p'_e	equivalent pressure on the intrinsic isotropic normal compression line
q	deviator stress
$q^* = q - q_0$	change in deviator stress from initial conditions
$S_\sigma = p'/p'_e$	stress sensitivity
S_u	undrained shear strength
t	time
α	viscosity parameter
β	rate-sensitivity coefficient
Γ	specific volume on the intrinsic compression line
ε	strain
ε_a	axial strain
ε_{vol}	volumetric strain
$\dot{\varepsilon}_a$	axial shearing strain-rate
$\dot{\varepsilon}_{after}$	final axial shearing strain-rate
$\dot{\varepsilon}_{before}$	initial axial shearing strain-rate
$\dot{\varepsilon}_c$	axial creep strain-rate
$\dot{\varepsilon}_a/\dot{\varepsilon}_c$	creep rate ratio
$\eta = q/p'$	effective stress ratio
λ	slope of normal compression line in $v - \ln p'$ space
σ'_{pc}	vertical preconsolidation pressure
σ'_a	axial effective stress
σ'_h	radial effective stress
$\dot{\sigma}_a$	rate of change of axial stress
v	specific volume
ϕ'	angle of shearing resistance

REFERENCES

Ackerley, S. K., Standing, J. R. & Hosseini Kamal, R. (2016). A system for measuring local radial strains in triaxial apparatus. *Géotechnique,* 66 (6)**,** 515-522.

Berre, T. & Bjerrum, L. (1973). Shear strength of normally consolidated clay. In *Proc. of the 8th International Conference on Soil Mechanics and Foundation Engineering*, Moscow, U.S.S.R., vol. 1, 39-49:

Bishop, A. W., Webb, D. L. & Lewin, P. I. (1965). Undisturbed samples of London Clay from the Ashford Common shaft: strength–effective stress relationships. *Géotechnique,* 15 (1)**,** 1-31.

Blight, G. (1964). The effect of nonuniform pore pressures on laboratory measurements of the shear strength of soils. *Laboratory shear testing of soils.* ASTM International.

Boudali, M., Leroueil, S. & Srinivasa Murthy, B. R. (1994). Viscous behaviour of natural clays. In *Proc. of the 13th International Conference on Soil Mechanics and Foundation Engineering*, New Delhi, India, vol. 1, 411-416:

Burland, J., Rampello, S., Georgiannou, V. & Calabresi, G. (1996). A laboratory study of the strength of four stiff clays. *Géotechnique,* 46 (3)**,** 491-514.

Casagrande, A. & Wilson, S. D. (1951). Effect of rate of loading on the strength of clays and shales at constant water content. *Géotechnique,* 2 (3)**,** 251-263.

Chandler, R. J., De Freitas, M. H. & Marinos, P. (2004). Geotechnical characterisation of soils and rocks: a geological perspective. In *Advances in geotechnical engineering: The Skempton conference: Proceedings of a three day conference on advances in geotechnical engineering, organised by the Institution of Civil Engineers and held at the Royal Geographical Society, London, UK, on 29–31 March 2004*, 67-102: Thomas Telford Publishing.

Chen, X. (2014). *Investigating intrinsic properties of London Clay.* Final-year undergraduate dissertation, Imperial College London.

Clayton, C. R. I. & Heymann, G. (2001). Stiffness of geomaterials at very small strains. *Géotechnique,* 51 (3)**,** 245-255.

Cotecchia, F. & Chandler, R. J. (1997). The influence of structure on the pre-failure behaviour of a natural clay. *Géotechnique,* 47 (3)**,** 523-544.

Cotecchia, F. & Chandler, R. J. (2000). A general framework for the mechanical behaviour of clays. *Géotechnique,* 50 (4)**,** 431-447.

Crooks, J. H. A. & Graham, J. (1976). Geotechnical properties of the Belfast estuarine deposits. *Géotechnique,* 26 (2)**,** 293-315.

Cuccovillo, T. & Coop, M. R. (1997). The measurement of local axial strains in triaxial tests using LVDTs. *Géotechnique,* 47 (1)**,** 167-171.

De Freitas, M. H. & Mannion, W. G. (2007). A biostratigraphy for the London Clay in London. *Géotechnique,* 57 (1)**,** 91-99.

Di Benedetto, H. & Tatsuoka, F. (1997). Small strain behavior of geomaterials: modelling of strain rate effects. *Soils and Foundations,* 37 (2)**,** 127-138.

Di Benedetto, H., Tatsuoka, F. & Ishihara, M. (2002). Time-dependent shear deformation characteristics of sand and their constitutive modelling. *Soils and Foundations,* 42 (2)**,** 1-22.

Gasparre, A., Hight, D. W., Coop, M. R. & Jardine, R. J. (2014). The laboratory measurement and interpretation of the small-strain stiffness of stiff clays. *Géotechnique,* 64 (12)**,** 942-953.

Gasparre, A., Nishimura, S., Coop, M. R. & Jardine, R. J. (2007). The influence of structure on the behaviour of London Clay. *Géotechnique,* 57 (1)**,** 19-31.

Graham, J., Crooks, J. H. A. & Bell, A. L. (1983). Time effects on the stress-strain behaviour of natural soft clays. *Géotechnique,* 33 (3)**,** 327-340.

Graham, J., Crooks, J. H. A. & Lau, S. L. K. (1988). Yield envelopes: identification and geometric properties. *Géotechnique,* 38 (1)**,** 125-134.

Hight, D., Bond, A. & Legge, J. (1992). Characterization of the Bothkennaar clay: an overview. *Géotechnique,* 42 (2)**,** 303-347.

Hight, D. W., Gasparre, A., Nishimura, S., Minh, N. A., Jardine, R. J. & Coop, M. R. (2007). Characteristics of the London Clay from the Terminal 5 site at Heathrow Airport. *Géotechnique,* 57 (1)**,** 3-18.

Hight, D. W., Mcmillan, F., Powell, J. J. M., Jardine, R. J. & Allenou, C. P. (2002). Some characteristics of London Clay. *Characterisation and engineering properties of natural soils,* 2 851-946.

Huggett, J. & Knox, R. O. B. (2006). Clay mineralogy of the Tertiary onshore and offshore strata of the British Isles. *Clay minerals,* 41 (1)**,** 5-46.

Jeong, S. W., Locat, J., Leroueil, S. & Malet, J.-P. (2010). Rheological properties of fine-grained sediment: the roles of texture and mineralogy. *Canadian Geotechnical Journal,* 47 (10)**,** 1085-1100.

King, C. (1981). The stratigraphy of London Basin and associated deposits. In *Tertiary research special paper*, 6, Rotterdam, the Netherlands: Backhuys:

Komoto, N., Tatsuoka, F. & Nishi, T. (2003). Viscous stress-strain properties of undisturbed Pleistocene clay and its constitutive modeling. In *Proc. 3rd International Conference on Pre-Failure Deformation Characteristics of Geomaterials*, Lyon, vol. 1, 579-587: Balkema.

Lade, P. V. (2016). *Triaxial testing of soils*: John Wiley & Sons.

Lambe, T. W. & Whitman, R. V. (1969). *Soil mechanics*, New York, USA: John Wiley & Sons.

Le, T. & Airey, D. (2021). Mechanical behaviour of a weakly structured soil at low confining stress. *Géotechnique*, doi: 10.1680/jgeot.21.00035.

Le, T., Airey, D. & Surjadinata, J. (2018). Modelling the behaviour of the Ballina test embankment. *Computers and Geotechnics*, 93 115-122.

Lefebvre, G. & Leboeuf, D. (1987). Rate effects and cyclic loading of sensitive clays. *Journal of Geotechnical Engineering*, 113 (5)**,** 476-489.

Leroueil, S. (2006). The isotache approach. Where are we 50 years after its development by Professor Šuklje? In *Proc. of the 13th Danube-European Conference on Geotechnical Engineering*, Ljubljana, Slovenia, vol. 1, 55-88:

Leroueil, S., Kabbaj, M., Tavenas, F. & Bouchard, R. (1985). Stress–strain–strain rate relation for the compressibility of sensitive natural clays. *Géotechnique*, 35 (2)**,** 159-180.

Leroueil, S., Tavenas, F., Samson, L. & Morin, P. (1983). Preconsolidation pressure of Champlain clays. Part II. Laboratory determination. *Canadian Geotechnical Journal*, 20 (4)**,** 803-816.

Leroueil, S. & Vaughan, P. R. (1990). The general and congruent effects of structure in natural soils and weak rocks. *Géotechnique*, 40 (3)**,** 467-488.

Locat, J. & Demers, D. (1988). Viscosity, yield stress, remolded strength, and liquidity index relationships for sensitive clays. *Canadian Geotechnical Journal*, 25 (4)**,** 799-806.

Momoya, Y., Ishii, T. & Tatsuoka, F. (1998). Strain rate-dependency of deformation of NC clay and prediction of undrained creep. In *Proc. of the 33rd Japan National Conference on Geotechnical Engineering*, Yamaguchi, vol. 1, 615-616 JGS.

Oka, F., Kodaka, T., Kimoto, S., Ishigaki, S. & Tsuji, C. (2003). Step-changed strain rate effect on the stress-strain relations of clay and a constitutive modeling. *Soils and Foundations*, 43 (4)**,** 189-202.

Pineda, J. A., Suwal, L. P., Kelly, R. B., Bates, L. & Sloan, S. W. (2016). Characterisation of Ballina clay. *Géotechnique*, 66 (7)**,** 556-577.

Qu, G., Hinchberger, S. D. & Lo, K. Y. (2010). Evaluation of the viscous behaviour of clay using generalised overstress viscoplastic theory. *Géotechnique*, 60 (10)**,** 777-789.

Richardson, A. M. & Whitman, R. V. (1963). Effect of strain-rate upon undrained shear resistance of a saturated remoulded fat clay. *Géotechnique*, 13 (4)**,** 310-324.

Sällfors, G. (1975). *Preconsolidation pressure of soft, high-plastic clays.* PhD thesis, Chalmers University of technology.

Smith, P. R. (1992). *The behaviour of natural high compressibility clay with special reference to construction on soft ground.* Imperial College, University of London.

Smith, P. R., Jardine, R. J. & Hight, D. W. (1992). The yielding of Bothkennar clay. *Géotechnique*, 42 (2)**,** 257-274.

Soga, K. & Mitchell, J. (1996). Rate-dependent deformation of structured natural clays. *In:* T. C. Sheahan & V. N. Kaliakin (eds.) *Measuring and modelling time-dependent soil behaviour.* Washington D.C.: ASCE.

Sorensen, K. K., Baudet, B. A. & Simpson, B. (2007). Influence of structure on the time-dependent behaviour of a stiff sedimentary clay. *Géotechnique*, 57 (1)**,** 113-124.

Sorensen, K. K., Baudet, B. A. & Simpson, B. (2010). Influence of strain rate and acceleration on the behaviour of reconstituted clays at small strains. *Géotechnique*, 60 (10)**,** 751-763.

Standing, J. R. (2020). Identification and implications of the London Clay Formation divisions from an engineering perspective. *Proceedings of the Geologists' Association*, 131 (5)**,** 486-499.

Šuklje, L. (1957). The analysis of the consolidation process by the isotaches method. In *Proc. of the 4th International Conference on Soil Mechanics and Foundation Engineering*, London, vol. 1, 200-206: Butterworths.

Tatsuoka, F., Di Benedetto, H., Enomoto, T., Kawabe, S. & Kongkitkul, W. (2008). Various viscosity types of geomaterials in shear and their mathematical expression. *Soils and Foundations*, 48 (1)**,** 41-60.

Tatsuoka, F., Ishihara, M., Di, B. H. & Kuwano, R. (2002). Time-dependent shear deformation characteristics of geomaterials and their simulation. *Soils and Foundations*, 42 (2)**,** 103-129.

Tatsuoka, F., Santucci De Magistris, F., Hayano, K., Koseki, J. & Momoya, Y. (2000). Some new aspects of time effects on the stress-strain behaviour of stiff geomaterials. A. Evangelista & L. Picarelli. In *The geotechnics of hard soils - soft rocks*, Naples, Italy, 1285-1371: Balkema, Rotterdam.

Tatsuoka, F. & Shibuya, S. (1992). Deformation characteristics of soils and rocks from field and laboratry tests. *Report of the Institute of Industrial Science, University of Tokyo;(Japan),* 37 (1).

Taylor, D. W. & Merchant, W. (1940). A theory of clay consolidation accounting for secondary compression. *Journal of Mathematics and Physics,* 19 (1-4)**,** 167-185.

Vaid, Y. P., Robertson, P. K. & Campanella, R. G. (1979). Strain rate behaviour of Saint-Jean-Vianney clay. *Canadian Geotechnical Journal,* 16 (1)**,** 34-42.

Wan, M. S. P., Standing, J. R., Potts, D. M. & Burland, J. B. (2017a). Measured short-term ground surface response to EPBM tunnelling in London Clay. *Géotechnique,* 67 (5)**,** 420-445.

Wan, M. S. P., Standing, J. R., Potts, D. M. & Burland, J. B. (2017b). Measured short-term subsurface ground displacements from EPBM tunnelling in London Clay. *Géotechnique,* 67 (9)**,** 748-779.

Table 1: Summary of soil properties

Soil	Depth below ground level [m]	Specific gravity	Plastic limit [%]	Liquid limit [%]
London Clay	LCUB21 (21.20-21.50)	2.75	24	79
	LCUB18 (18.06-18.36)	2.76	25	78
Ballina clay	6.4-7.0	2.68	43	118
Gypsum (hydrated calcium sulfate)	--	2.39	non-plastic	62
Kaolin	--	2.64	24	55

Table 2: Summary of triaxial compression tests on intact samples with stepwise changes in axial strain-rate

	London Clay		Ballina clay		Gypsum-kaolin			
	LCUB21	LCUB18	BC6.7VS1	BC6.7VS2	GKVS03	GKVS04	ICGKVS01	ICGKVS02
Stress state prior to shearing (p', q) [kPa]	$(311, -130)$	$(246, -106)$	(23,14)	(40,0)	(40,0)	(40,0)	(40,0)	(40,0)
e_0	0.70	0.72	3.16	3.06	1.62	1.63	1.56	1.57
Consolidation strain, ε_{vol} [%]	0.21†	0.16†	2.24‡	3.01‡	0.92‡	0.64‡	0.09†	0.22†
Coefficient of consolidation, c_v [m^2/year]	0.93*	0.84*	5.50*		8.40			
Axial creep strain-rate, $\dot{\varepsilon}_c$ [%/hr]	0.0002	0.0001	0.002	0.004	0.005	0.004	0.0002	0.0001
Applied axial stress rate, $\dot{\sigma}_a$ [kPa/hr]	0.67, 1.29	3.30	-	-	-	-	-	0.90, 4.94, 9.51
Axial shearing strain-rate, $\dot{\varepsilon}_a$ [%/hr]	0.002, 0.02, 0.2	0.01, 0.02,0.2	0.5,5.0,50.0	0.5,5.0,50.0	0.5,5.0,50.0	0.5,5.0,50.0	0.5,5.0,50.0	0.5,5.0,50.0

†Based on volumetric deformations calculated from local strain measurements
‡Based on volumetric deformations calculated from volume gauge measurements
*Determined based on oedometer tests on nearby samples

Table 3: Summary of triaxial compression tests on reconstituted samples with stepwise changes in axial strain-rate

	London Clay	Ballina clay	Gypsum-kaolin	
	rLCUB23	rBC6.7VS	rGK	rGKVS
Stress state prior to shearing (p', q) [kPa]	(400,0)	(40,0)	(40,0)	(40,0)
e_0	1.10	2.67	1.29	1.24
Consolidation strain, ε_{vol} [%]	11.2†	3.7‡	1.7‡	0.6‡
Coefficient of consolidation, c_v [m^2/year]	0.26	0.52	1.94	
Gradient of intrinsic ICL, λ	0.17	0.33	0.14	
Intercept of intrinsic ICL at 1kPa, Γ	2.90	3.75	1.75	
Axial creep strain-rate [%/hr]	0.0003	0.007	0.004	0.004
Axial shearing strain-rate [%/hr]	0.002, 0.02, 0.2	0.5,5.0,50.0	5.0	0.5,5.0,50.0

†Based on volumetric deformations calculated from local strain measurements
‡Based on volumetric deformations calculated from volume gauge measurements

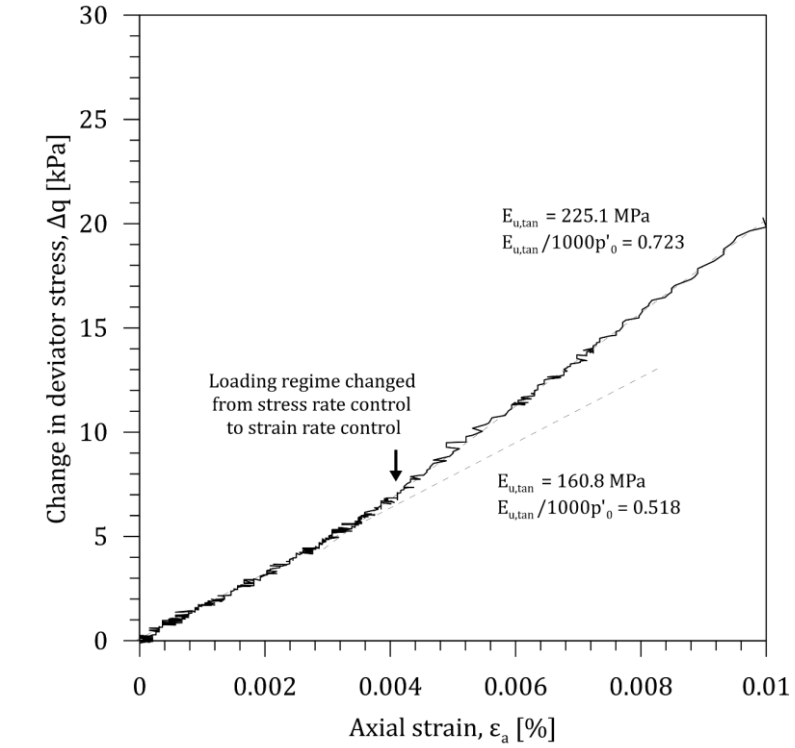

(a)

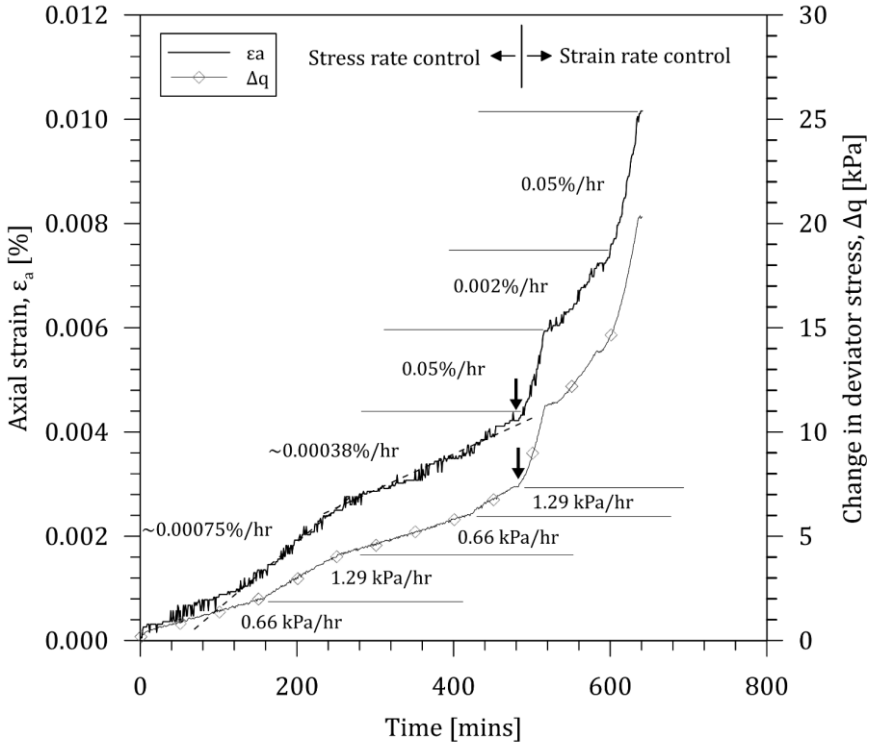

(b)

Figure 1 Very small strain region for undrained compression on Sample LCUB21.
(a) Change in deviator stress-strain response and (b) change in deviator stress and axial strain measured against time

during undrained compression

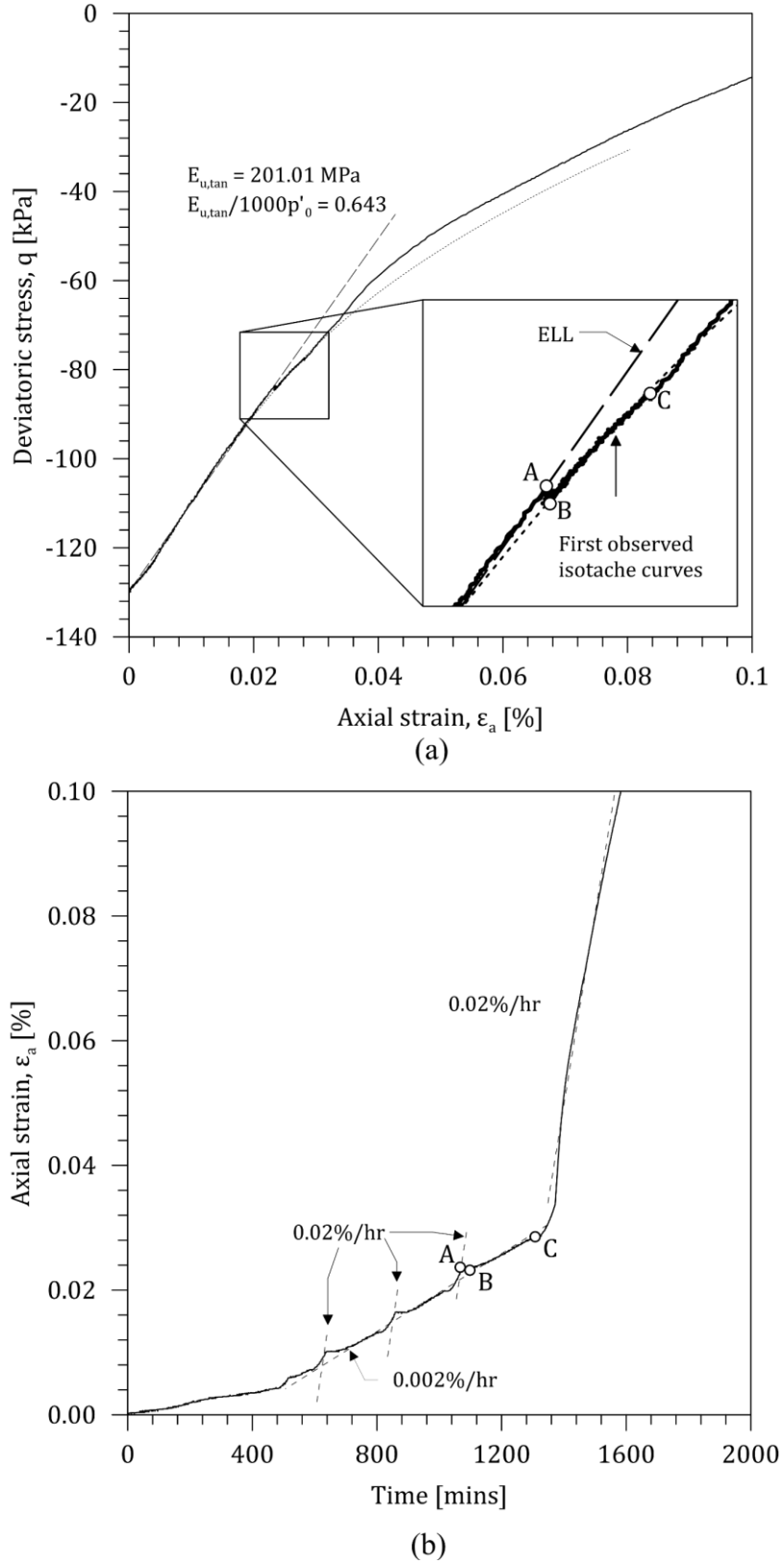

Figure 2 Small strain region for undrained compression on Sample LCUB21. (a) Deviator stress-strain response and (b) axial strain measured against time during

undrained compression

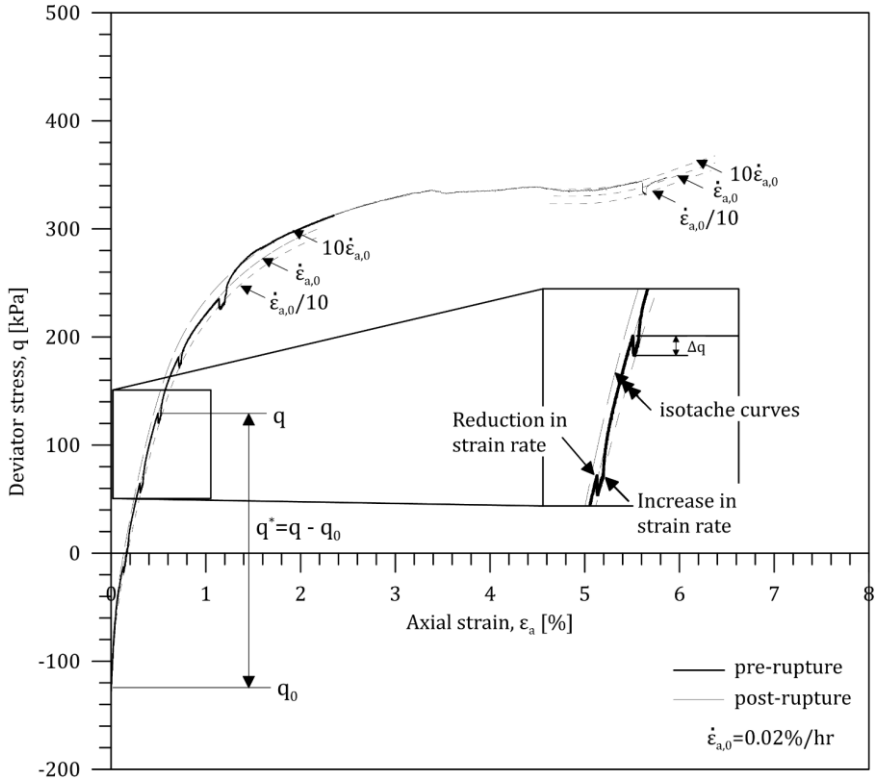

Figure 3 Full stress-strain response of Sample LCUB21 sheared undrained to failure with stepwise changes in strain-rate

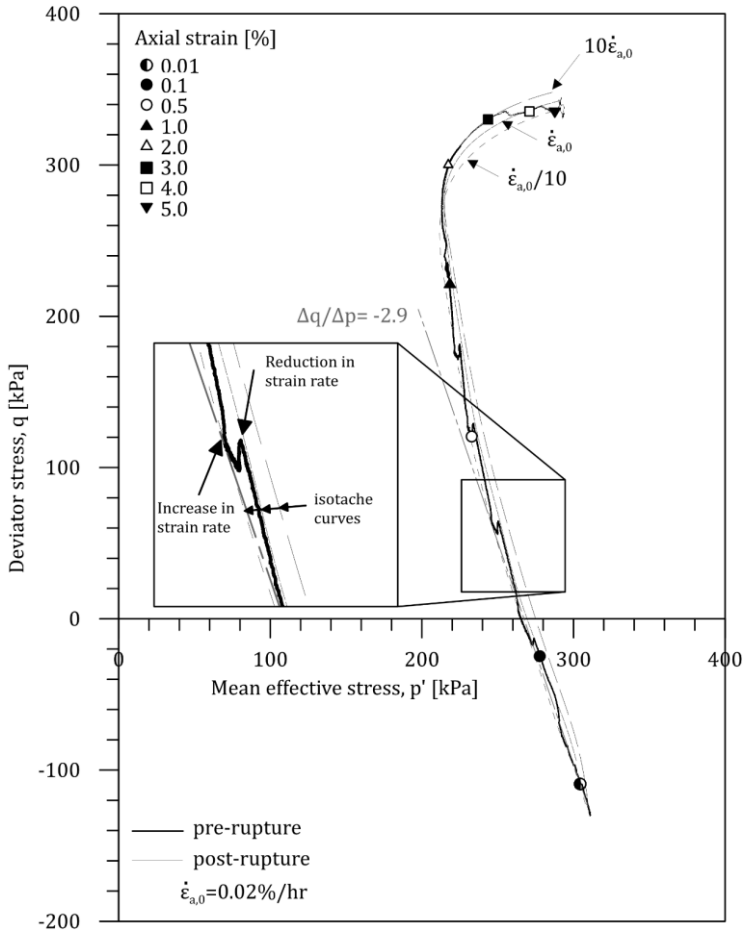

Figure 4 Effective stress path of Sample LCUB21 sheared undrained to failure with stepwise changes in strain-rate

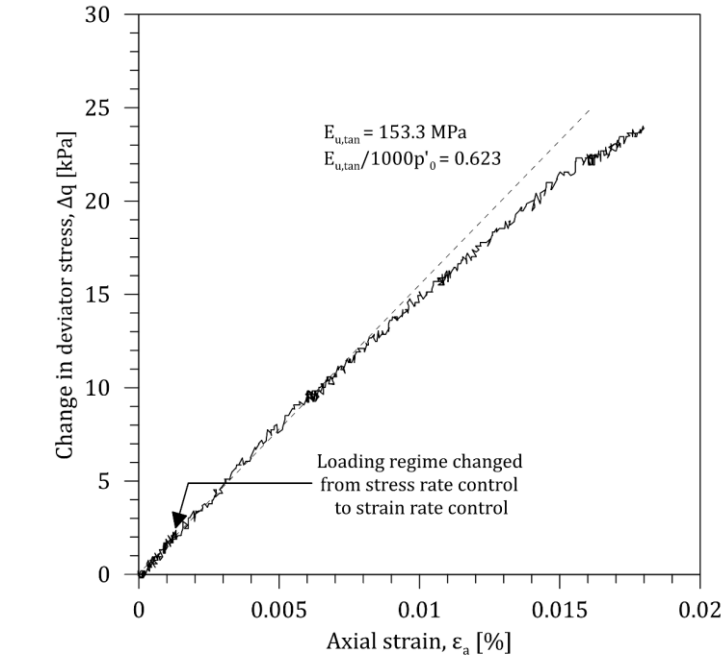

(a)

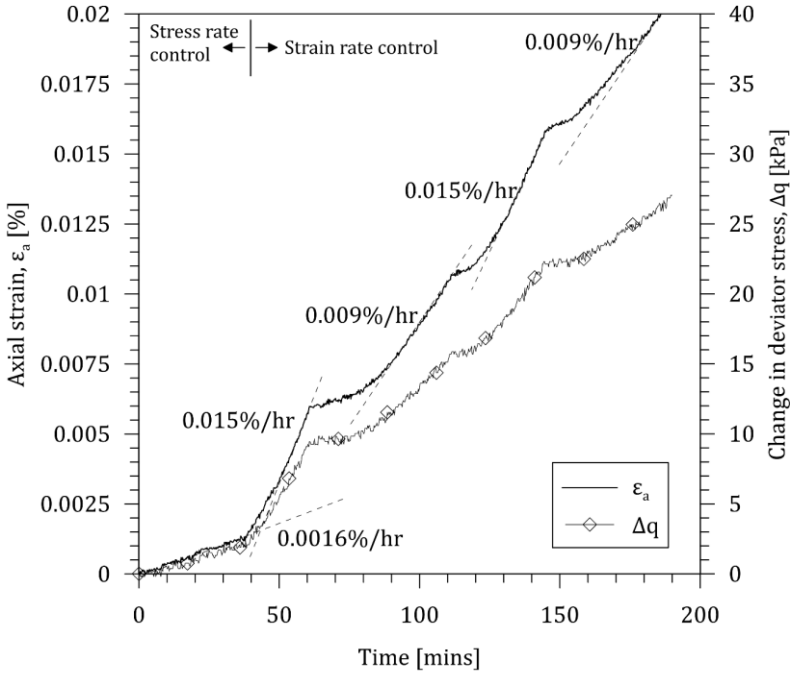

(b)

Figure 5 Very small strain region for undrained compression on Sample LCUB18.
(a) change in deviator stress-strain response and (b) change in deviator stress and axial strain measured against time during undrained compression

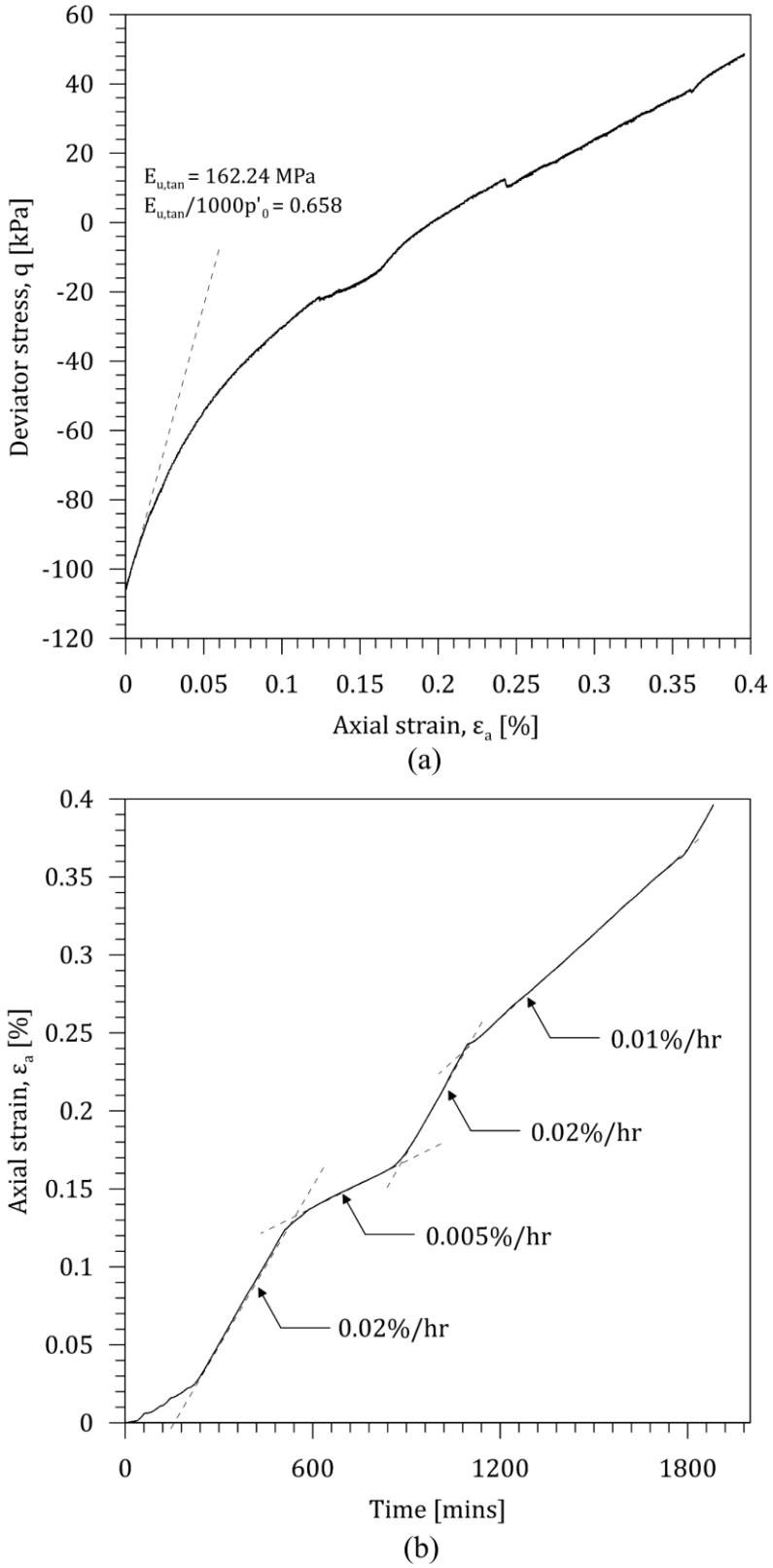

Figure 6 Small strain region for undrained compression on Sample LCUB18. (a) deviator stress-strain response and (b) axial strain measured against time during undrained compression

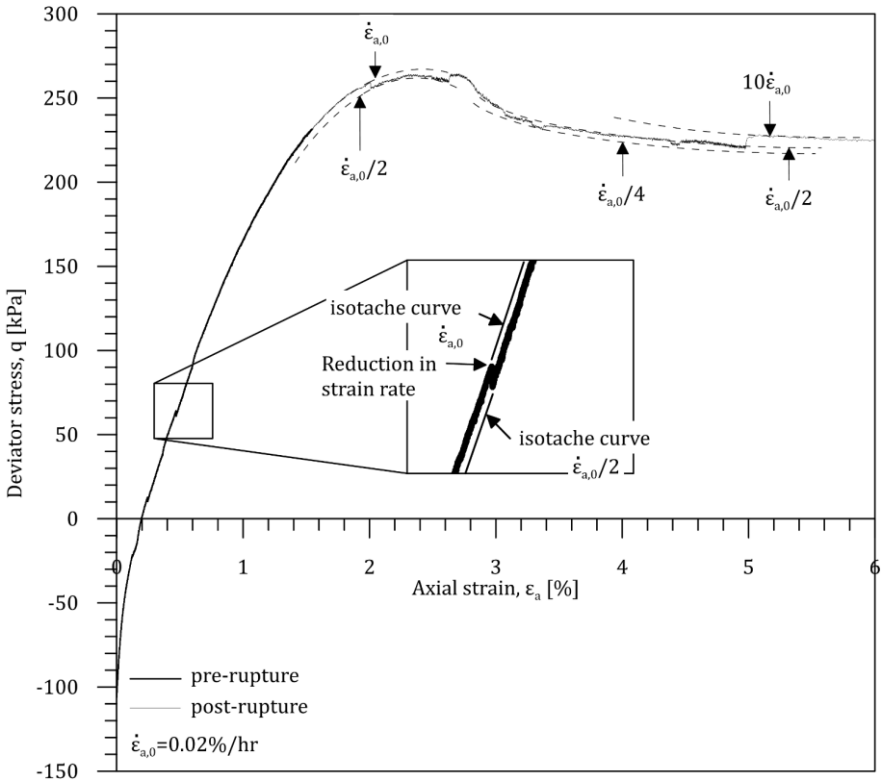

Figure 7 Full stress-strain response of Sample LCUB18 sheared undrained to failure with stepwise changes in strain-rate

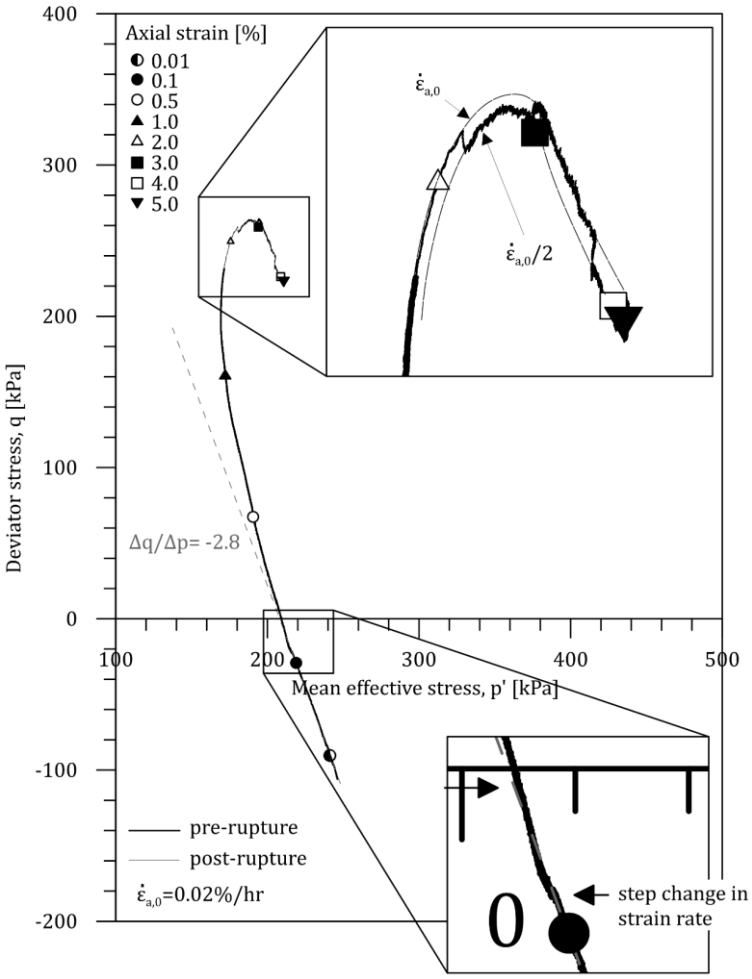

Figure 8 Effective stress path of Sample LCUB18 sheared undrained to failure with stepwise changes in strain-rate

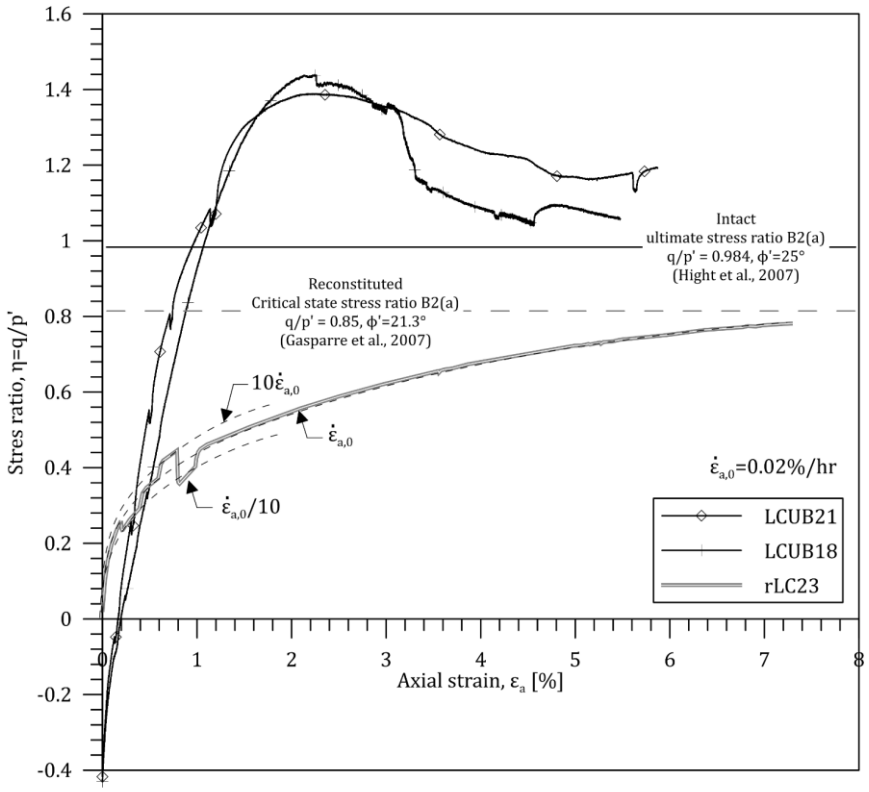

Figure 9 Effective stress ratio for London Clay samples from Division B2 subjected to stepwise changes in strain-rate

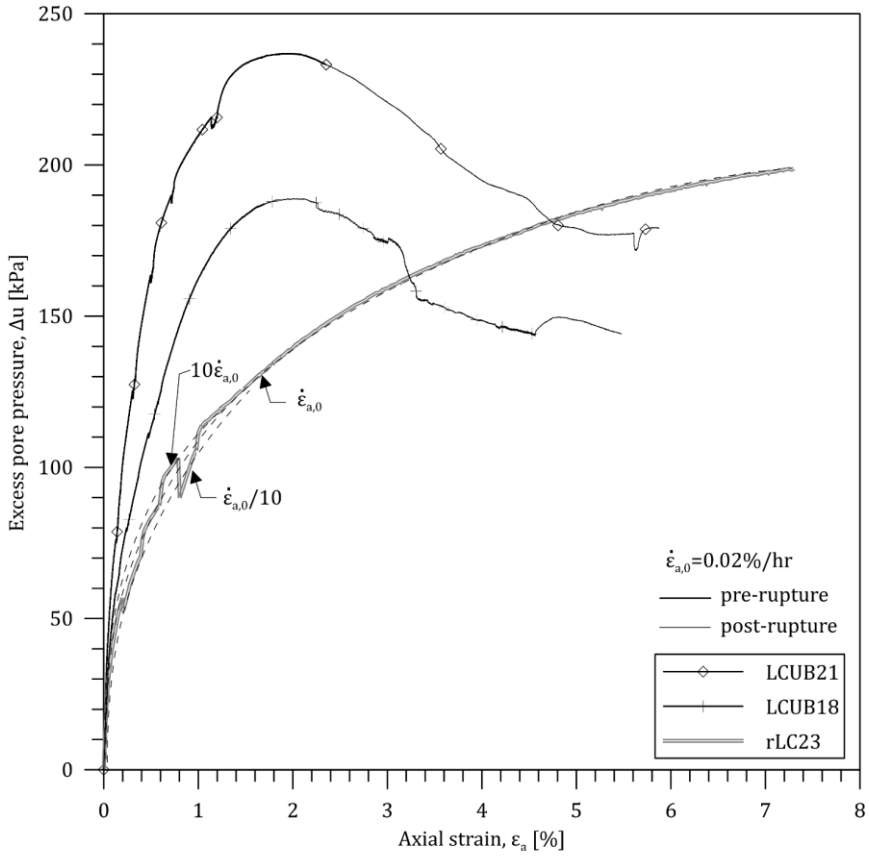

Figure 10 Effect of strain rate on excess pore pressure generation for London Clay samples from Division B2

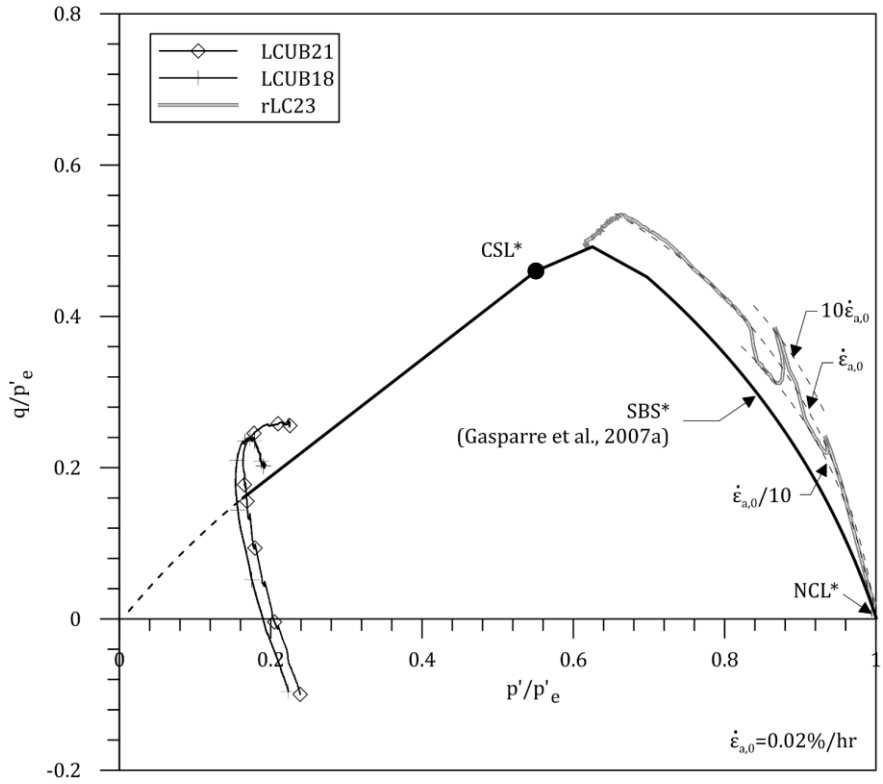

Figure 11 Normalised stresses paths for London Clay samples from Division B2

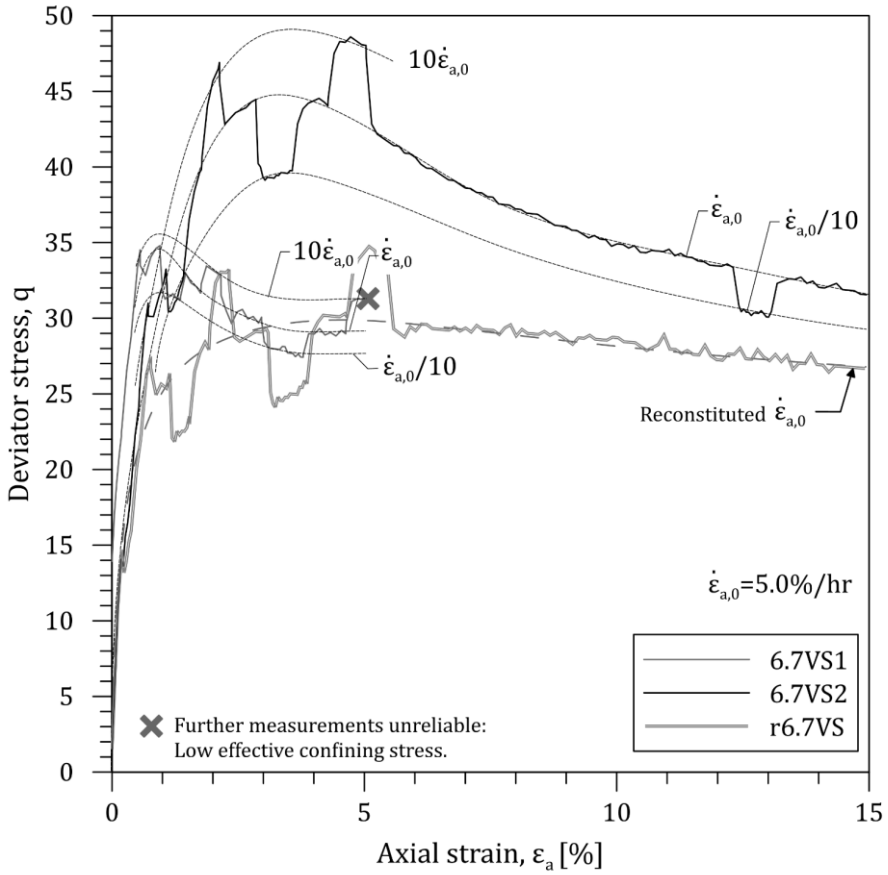

Figure 12 Stress-strain curves for stepwise strain-rate tests on Ballina clay

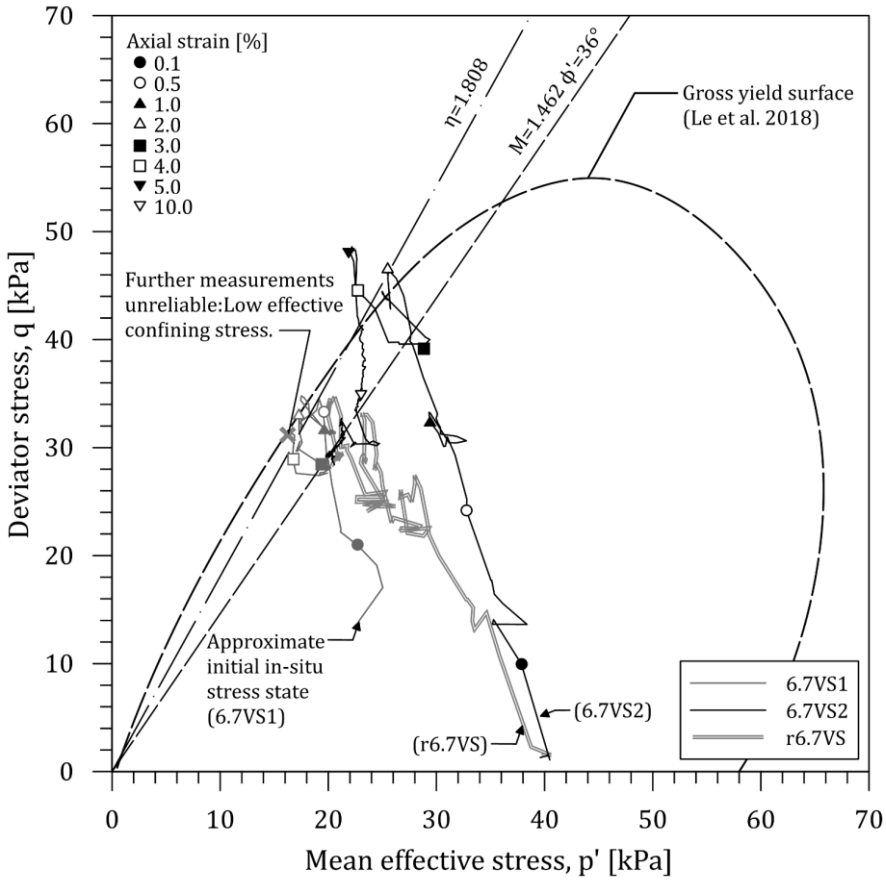

Figure 13 Effective stress paths for stepwise changes in strain-rate-tests Ballina clay: strain-rates 0.5, 5.0, 50%/hour

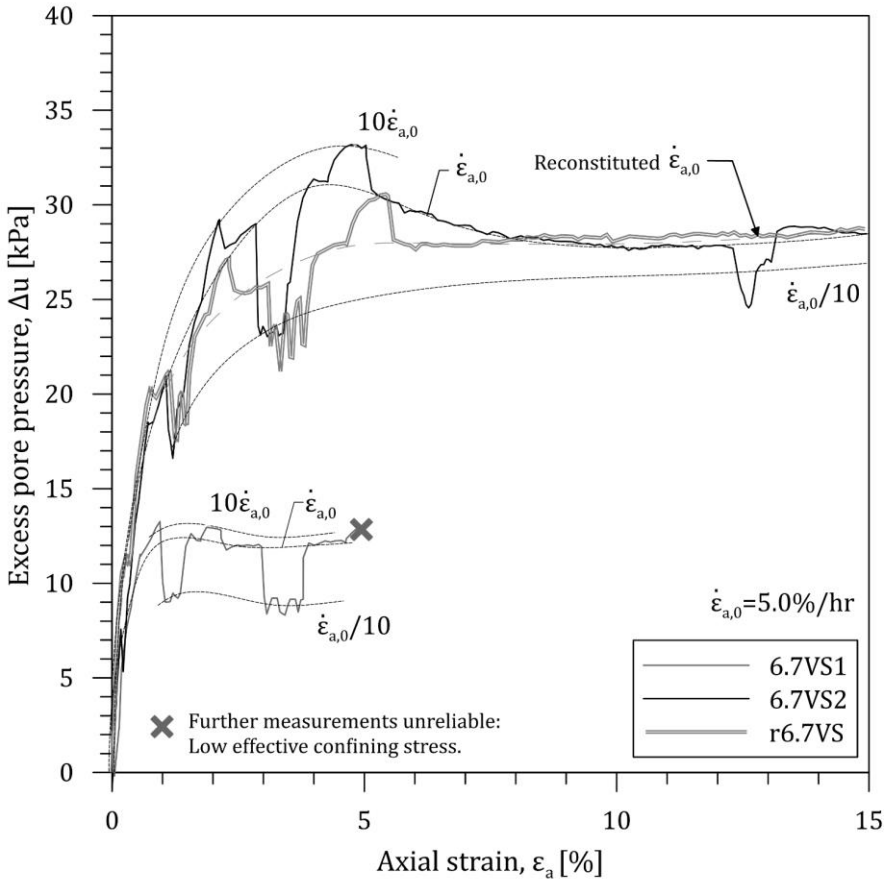

Figure 14 Effect of strain rate on excess pore pressure response during undrained compression of Ballina clay

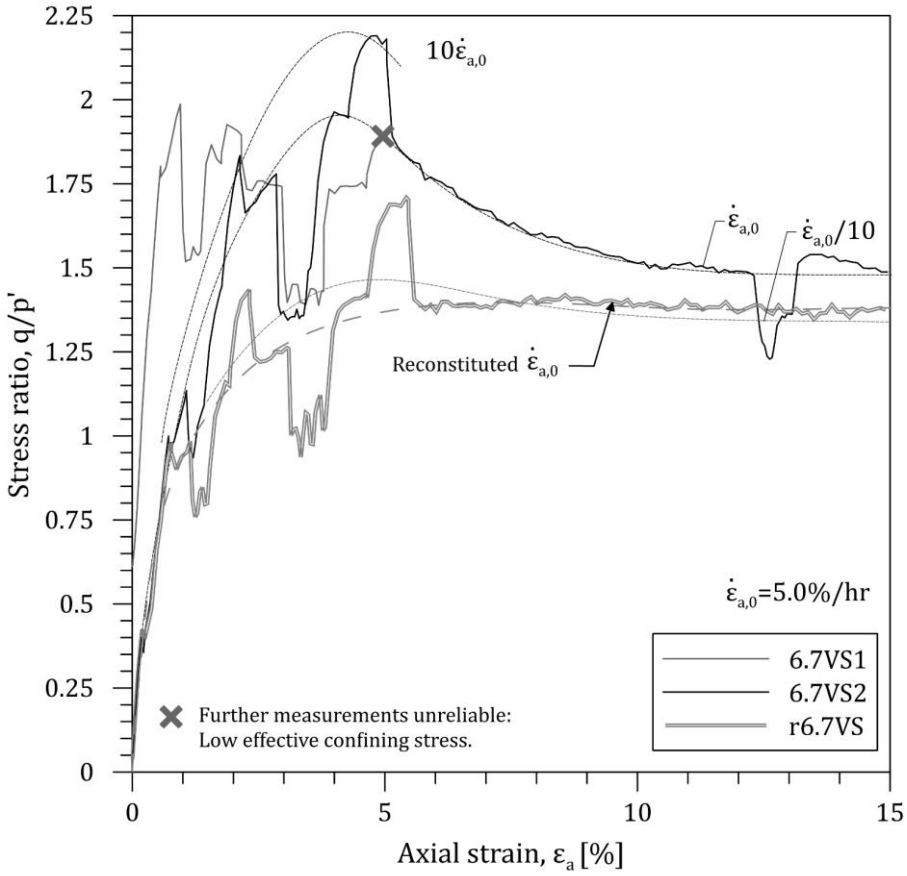

Figure 15 Effective stress ratio for undisturbed and reconstituted samples of Ballina clay subjected to stepwise changes in strain-rate

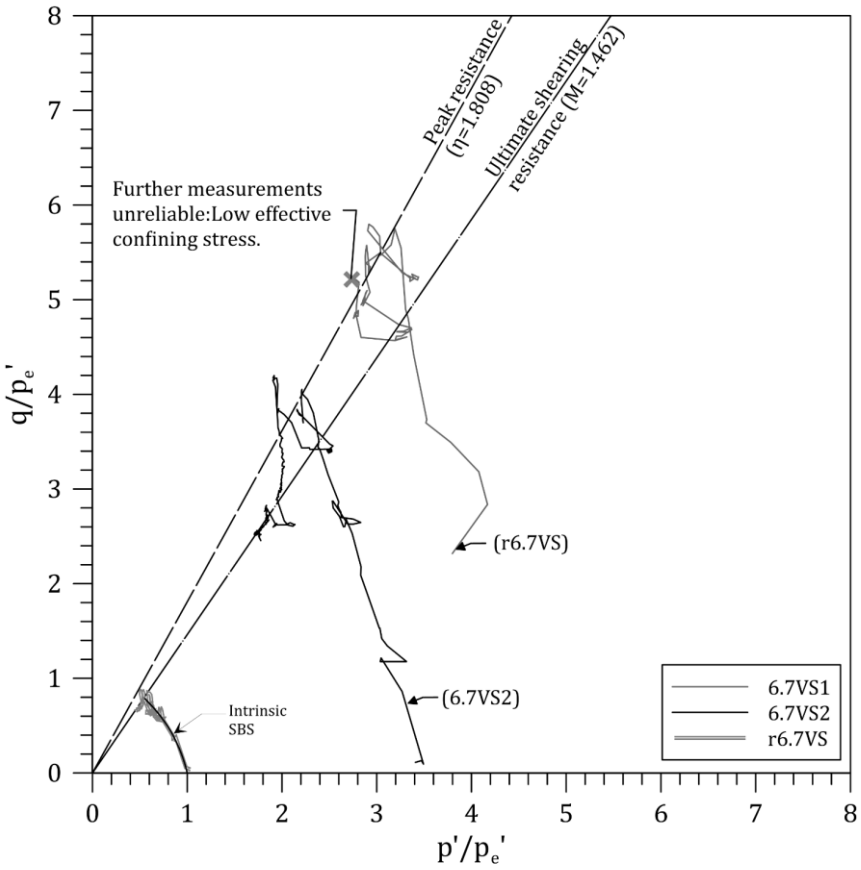

Figure 16 Normalised stress paths for natural and reconstituted samples of Ballina clay

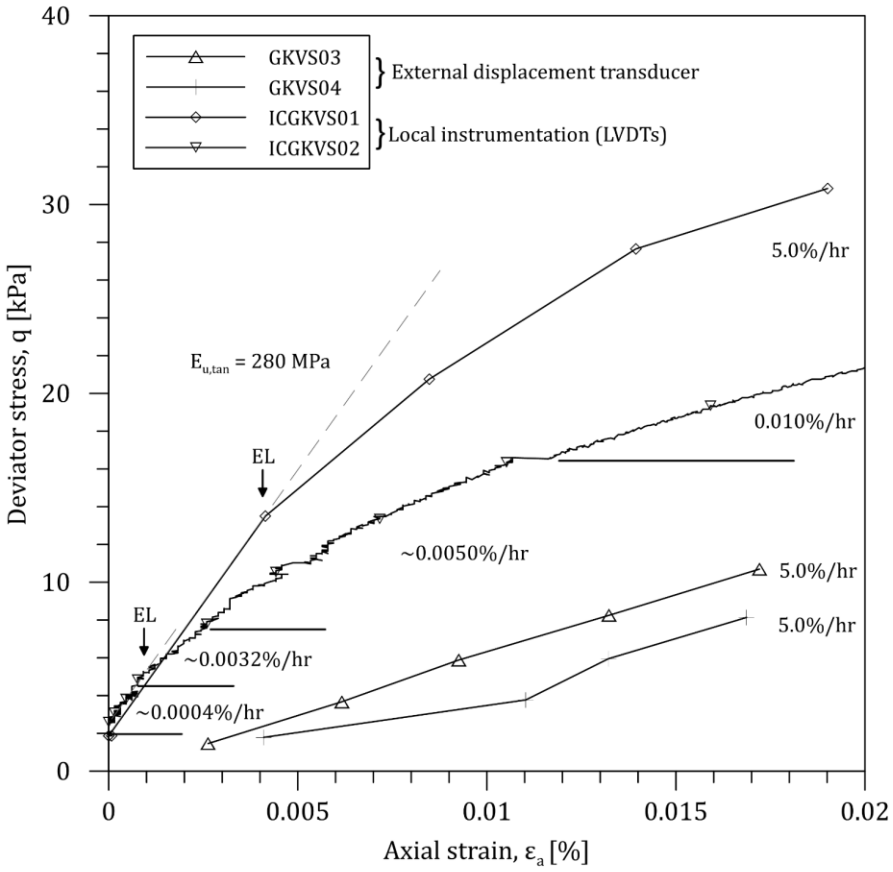
GKVS03
GKVS04
ICGKVS01
ICGKVS02
External displacement transducer
Local instrumentation (LVDTs)
Deviator stress, q [kPa]
Axial strain, ε_a [%]
E_u,tan = 280 MPa
EL
EL
~0.0032%/hr
~0.0004%/hr
~0.0050%/hr
0.010%/hr
5.0%/hr
5.0%/hr
5.0%/hr
0
10
20
30
40
0
0.005
0.01
0.015
0.02

(a)

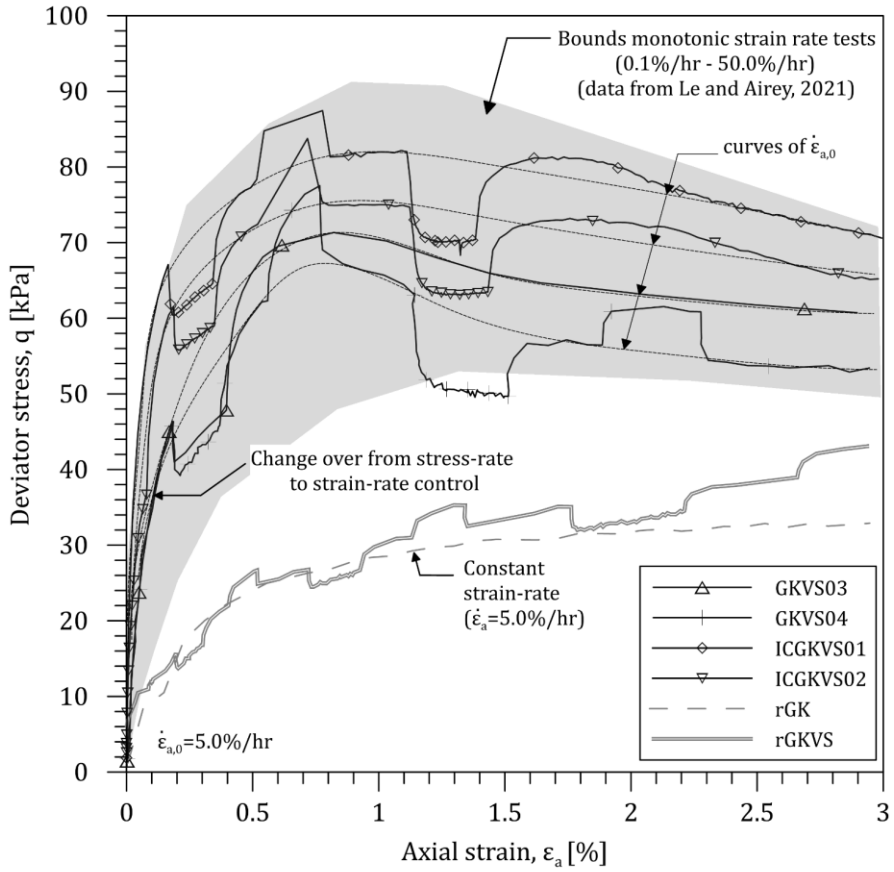

(b)

Figure 17 Stress-strain curves for stepwise strain-rate tests on gypsum-kaolin specimens (a) at small-strains and (b) large strains

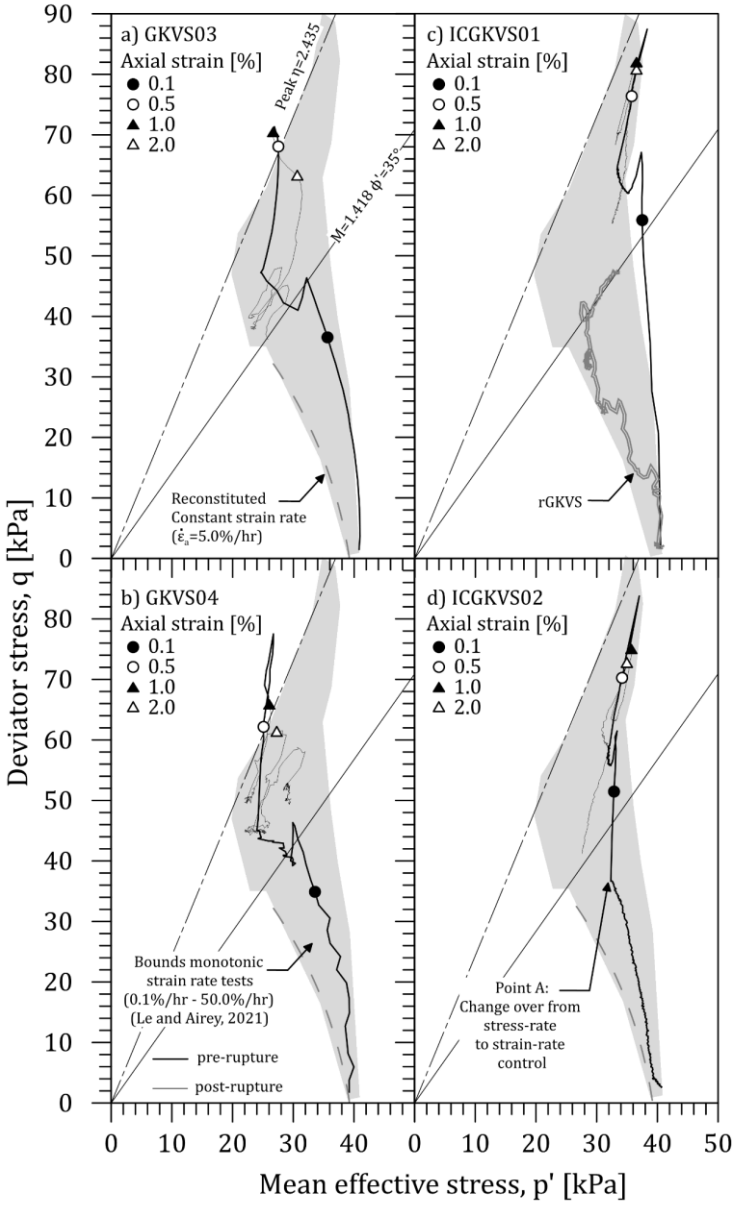

Figure 18 Effective stress path for stepwise changes in strain-rate-tests gypsum-kaolin specimens: strain-rates 0.5,5.0,50%/hour

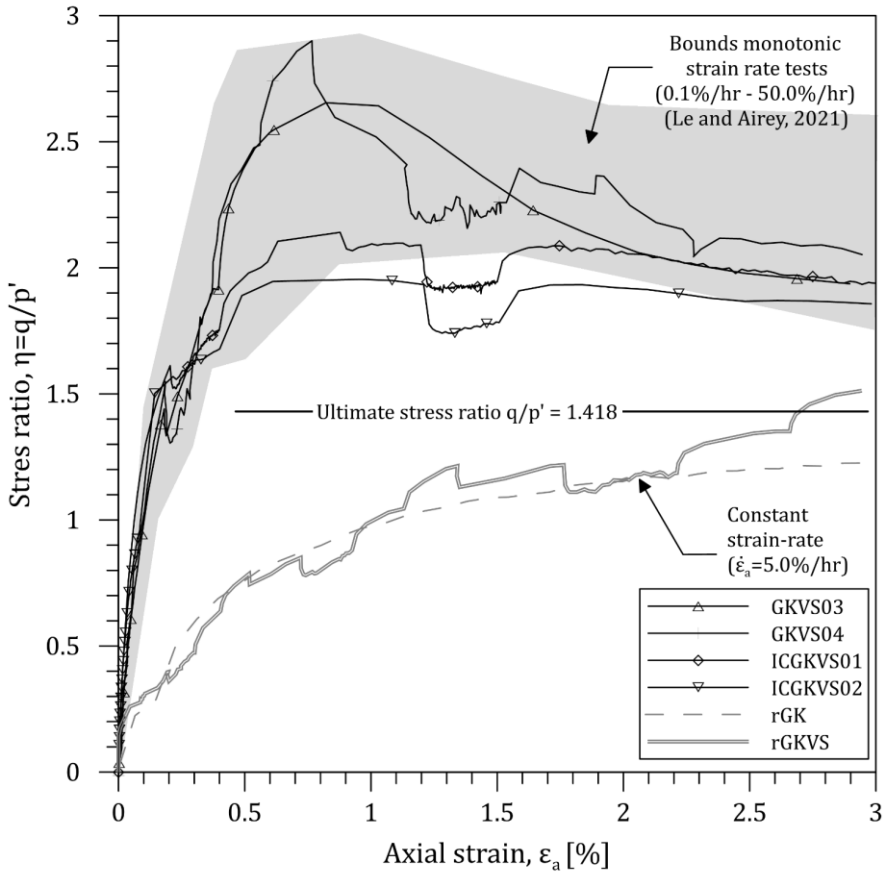

Figure 19 Effective stress ratio for tests on gypsum-kaolin specimens subject to stepwise change in strain-rate

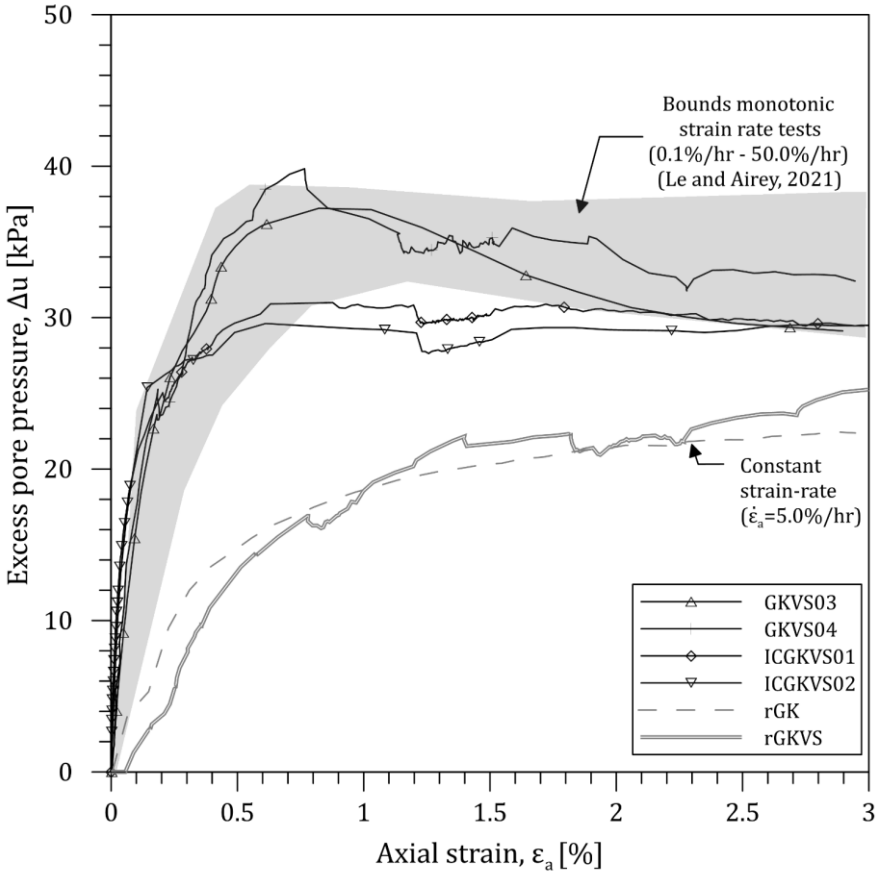

Figure 20 Effect of strain rate on excess pore pressure response during undrained compression of gypsum-kaolin specimens

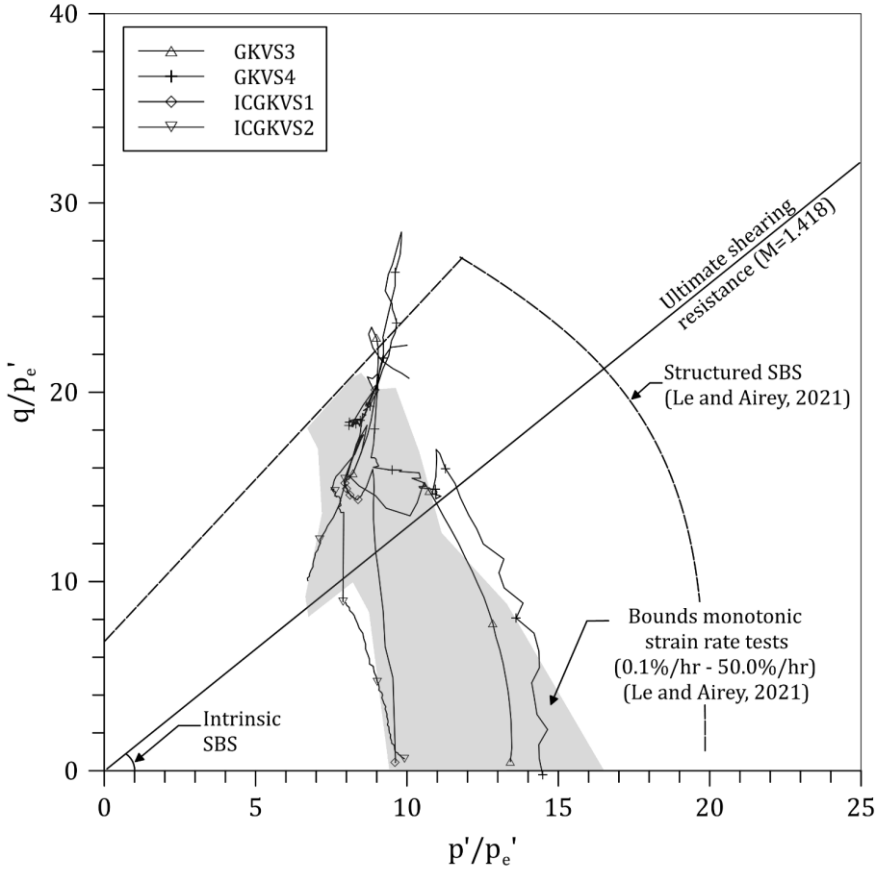

Figure 21 Normalised stresses paths for intact and reconstituted gypsum-kaolin specimens

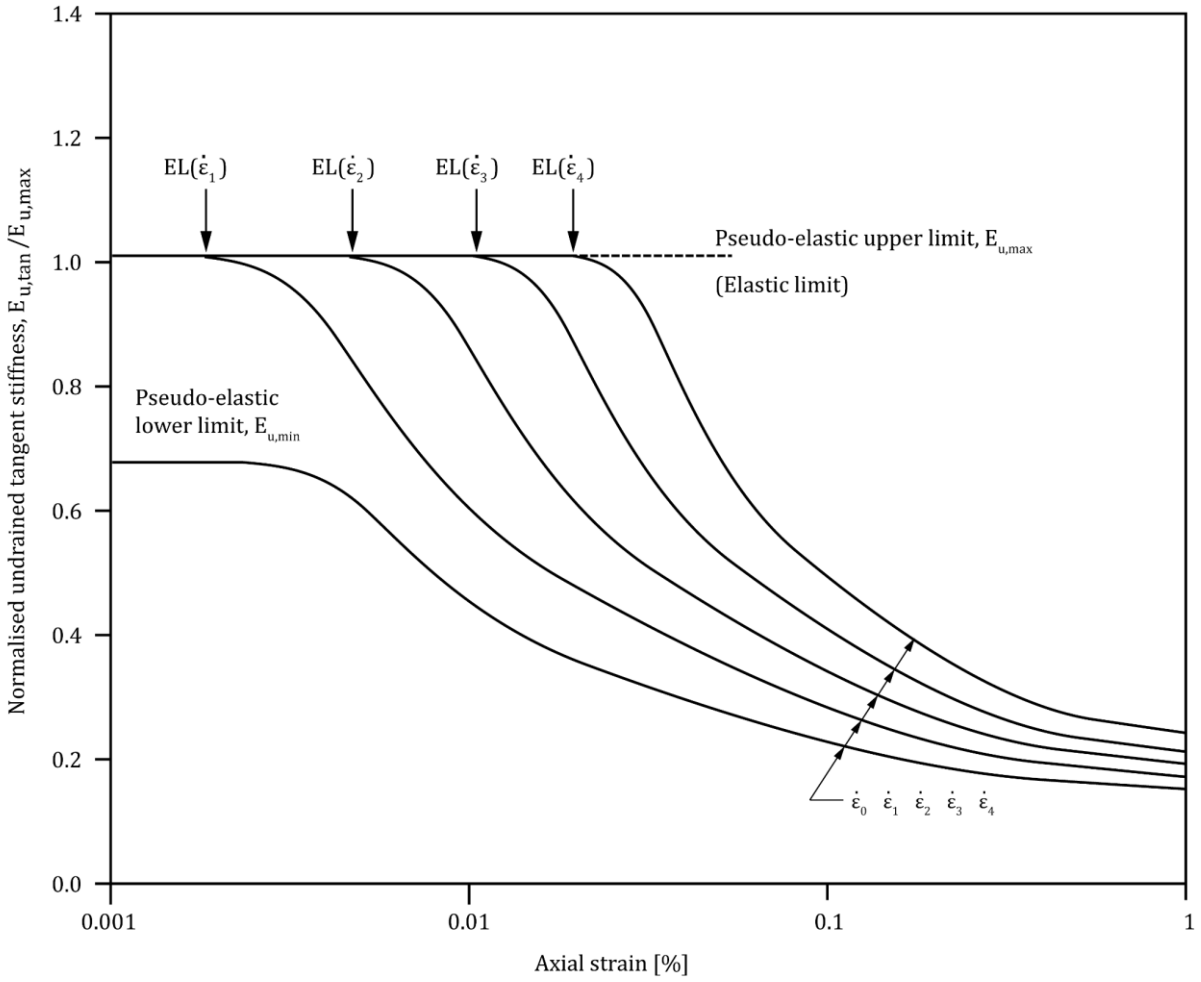

Figure 22 Diagram of stiffness decay curve for tests with different constant strain-rate
10

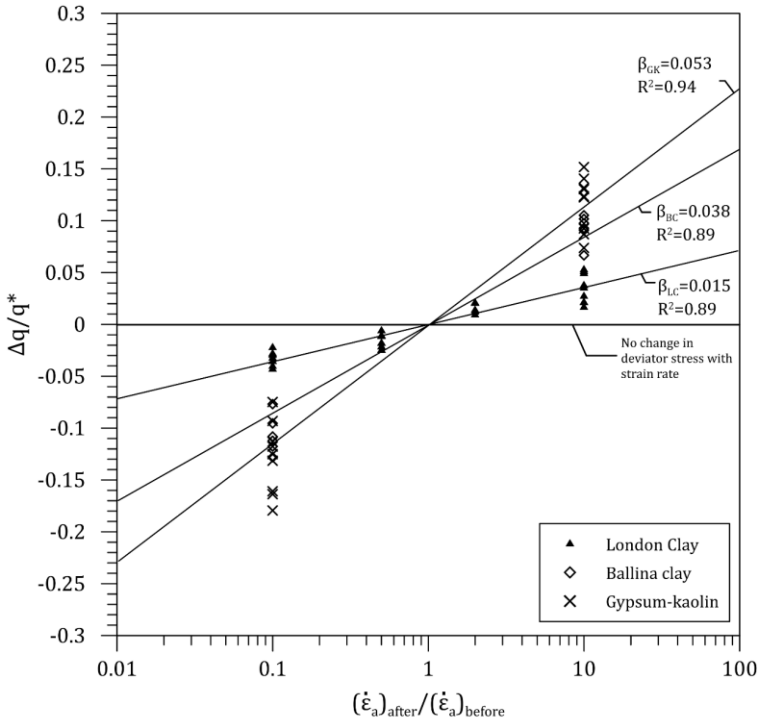

(a)

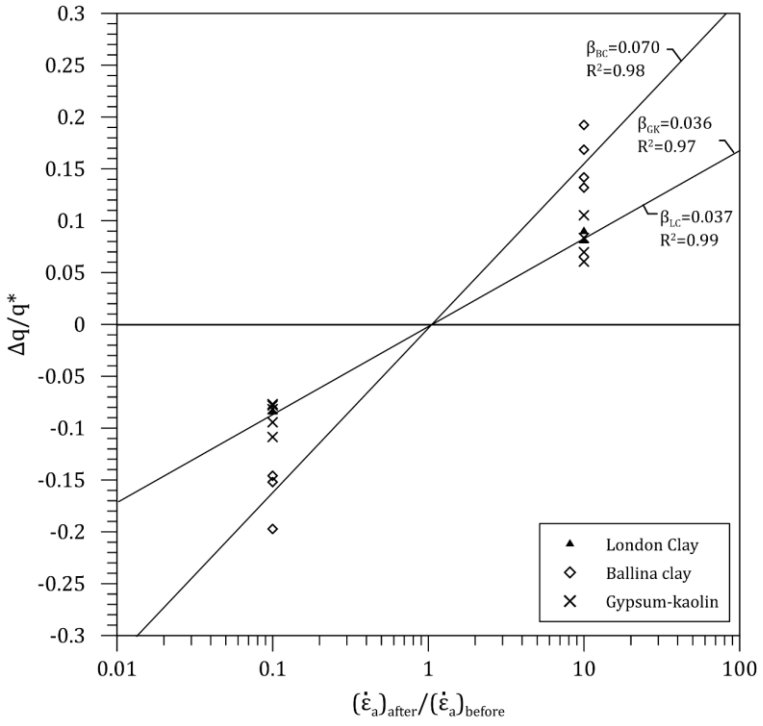

(b)

Figure 23 Viscous parameter β for structured soils in the (a) intact and (b) reconstituted state.

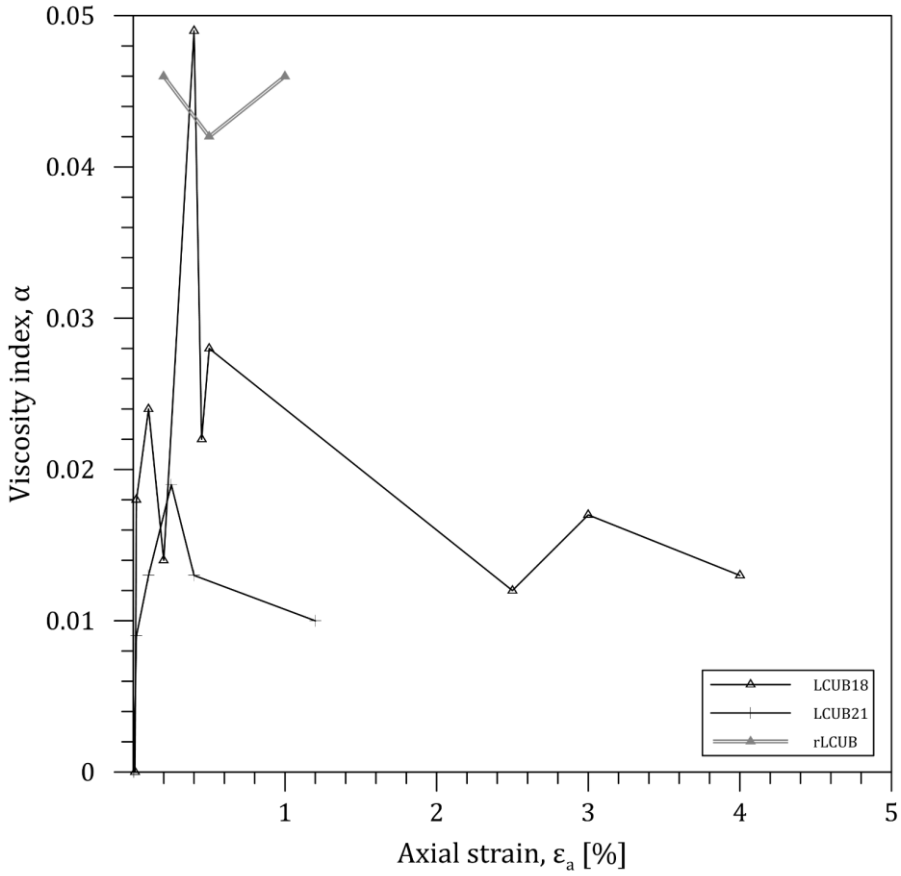

Figure 24 Evolution of rate sensitivity parameter α for London Clay

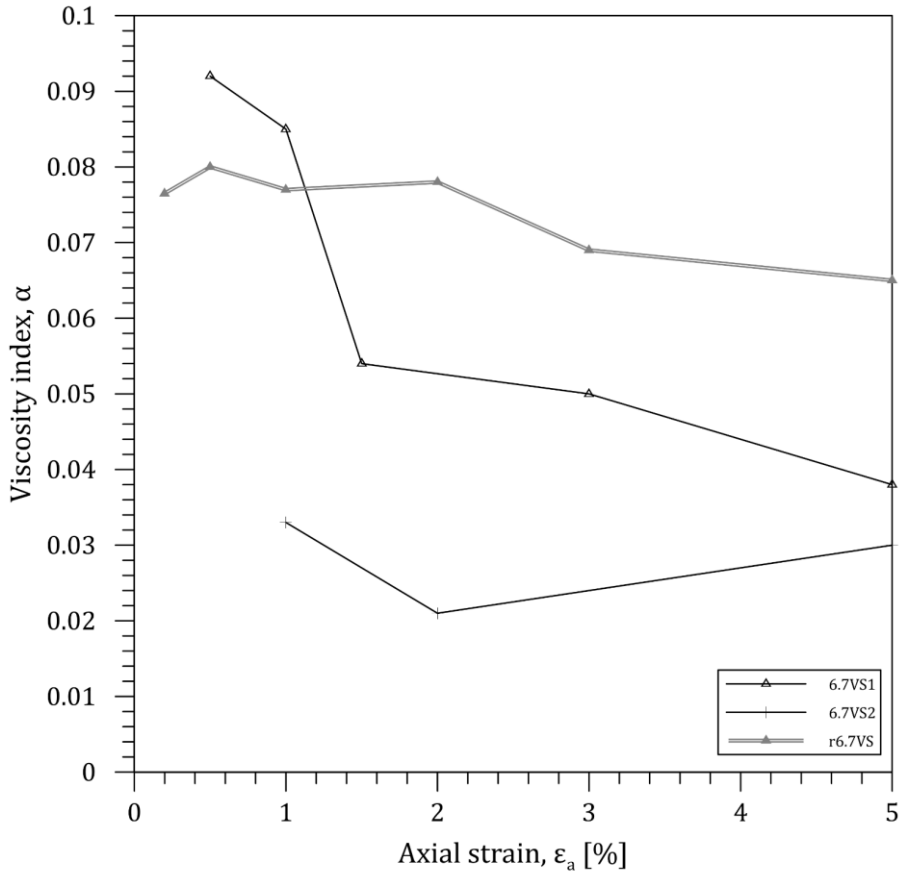

Figure 25 Evolution of rate sensitivity parameter α for Ballina clay

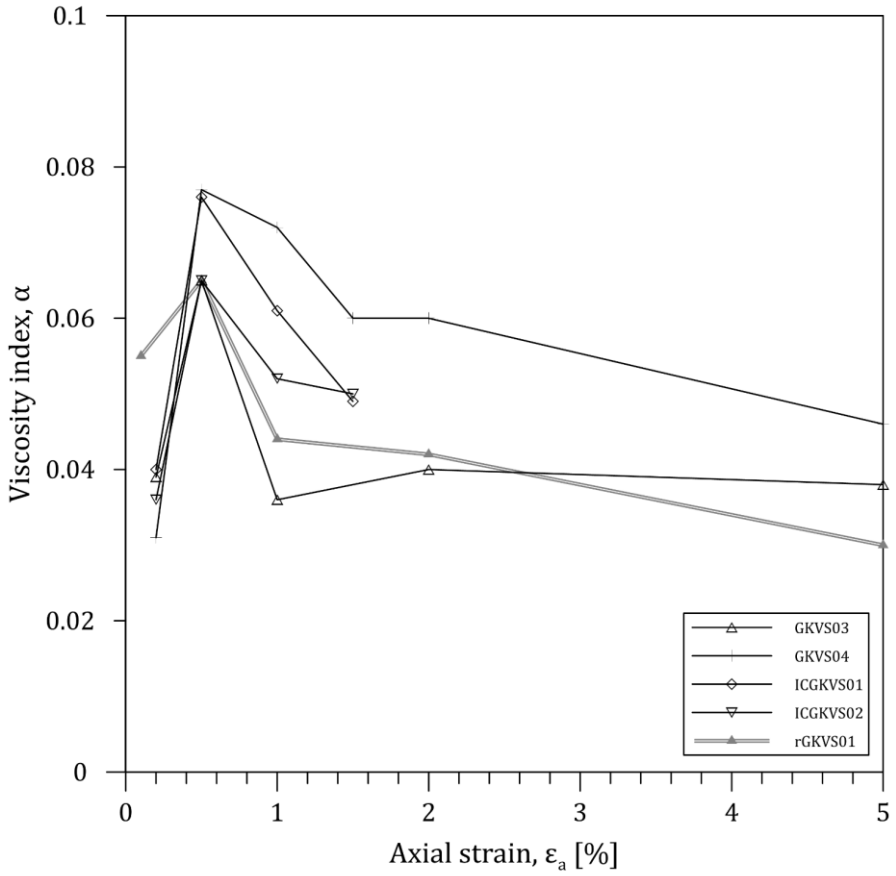

Figure 26 Evolution of rate sensitivity parameter α for gypsum-kaolin specimens